Soil Dynamics and Earthquake Engineering 195 (2025) 109413

Contents lists available at ScienceDirect

Soil Dynamics and Earthquake Engineering

journal homepage: www.elsevier.com/locate/soildyn

Experimental and empirical shear modulus reduction curves for a wide range of strains

P. Anbazhagan [a,*], Kunjari Mog [b], Mir Zeeshan Ali [a], B Sai Laxman [a]

[a] Department of Civil Engineering, Indian Institute of Science, Bangalore, 560012, India
[b] Department of Civil Engineering, National Institute of Technology, Hamirpur, H.P, 177005, India

ARTICLE INFO

Keywords:
Shear modulus reduction
Asymmetric hysteresis loop
Resonant column
Cyclic triaxial
Reference strain
Soil dynamics

ABSTRACT

Understanding the shear modulus reduction behavior of soils under varying strain levels is vital for predicting soil response during seismic events. This study investigates the shear modulus reduction of diverse soil types using combined resonant column and cyclic triaxial tests. A single specimen is employed for both small and large strain ranges, which differs from conventional approaches that utilize two separate specimens. The shear modulus is assessed using different elastic moduli (E_1, E'_1, E_2, and E_3) within the stress-strain hysteresis loop, considering both compressional and extensional cyclic loadings. Results show significant deviation in secant moduli (G_1, G'_1, G_2, and G_3), varying from less than 20 % at small strains to 25–130 % at large strains, with hysteretic behavior becoming more asymmetrical at higher shear strains. Confining pressure (CP), relative density (RD), and coefficient of uniformity (C_U) are identified as critical factors influencing modulus reduction. A two-parameter model was developed to accurately capture the strain-dependent normalized shear modulus behavior. Parameter '*a*' is found to be independent of RD, CP, and C_U, while reference strain 'γ_{ref}' shows a strong dependency on confining pressure with an indeterminate relationship with relative density. Poorly graded soils exhibit higher stiffness with greater 'γ_{ref}' values. The newly proposed mean, upper and lower bound curves can predict normalized shear modulus up to 10 % shear strains, significantly enhancing predictive capabilities beyond the typical 1 % strain limits of existing models. This improvement provides a more accurate basis for seismic response analysis, particularly in regions with similar soil types.

1. Introduction

Strain-dependent dynamic properties, such as shear modulus (G) and damping ratio (D), are crucial for analysing soil-structure interactions and conducting site-specific ground response analyses. Shear modulus measures soil stiffness against shear-induced deformations, while the damping ratio represents energy dissipation in soil. These properties are influenced by parameters, including shear strain, confining pressure, plasticity index, grain size distribution, loading duration and frequency, number of loading cycles, relative density or void ratio, degree of saturation, and over-consolidation ratio [1–6].

Despite the frequent occurrence of significant earthquakes and associated geotechnical hazards in the Himalayan region, there is a notable lack of established shear modulus reduction, and damping curves tailored to the region's diverse soil types. The complex geological formations of several parts of Himalaya limit the applicability of generic models, such as G/Gmax-log γ and D-log γ [7]. Consequently, developing soil-specific models is essential for accurately estimating site-specific earthquake ground motion hazards [8,9]. Previous research demonstrates that shear modulus decreases, and damping ratio increases with increasing shear strains [1,2,10–14]. At very small strains, these properties remain constant, known as small strain shear modulus (G_{max}) and small strain damping ratio (D_{min}). Beyond a threshold strain, soils exhibit non-linear behavior with decreased shear modulus and increased damping ratio. Higher confining pressure shifts the G curve rightward and the D curve downward, indicating less reduction in modulus and a lesser increase in energy dissipation at large strains [2,15]. Similarly, increased plasticity shifts the G curve rightward and the D curve downward [3,4]. The coefficient of uniformity (C_U) shifts the G curve leftward, leading to greater modulus degradation [13,16].

In geotechnical practice, the small strain shear modulus (<0.01 %) is typically determined by measuring V_S in the field or through low-strain laboratory tests, such as resonant column and bender element tests. For medium to large strains (0.01–1 %), torsional shear and cyclic triaxial

* Corresponding author.
E-mail address: anbazhagan@iisc.ac.in (P. Anbazhagan).

https://doi.org/10.1016/j.soildyn.2025.109413
Received 21 August 2024; Received in revised form 13 March 2025; Accepted 31 March 2025

tests are employed. Data from these tests are usually combined to create a comprehensive shear modulus profile across a wide strain range, which is then normalized with G_{max} to generate a normalized shear modulus curve. These normalized shear modulus degradation curves (G/Gmax-log γ) and damping ratio curves (D-log γ) are used in seismic response analysis software such as SHAKE, D-MOD2000, and DEEPSOIL [17–19]. However, combining data from different tests and specimens introduces variability due to differences in soil fabric and state, increasing costs and resource requirements. Empirical equations [2,11,13,20] supplement experimental data (typically up to 1 % strain) with extrapolations but require multiple specimens, as measuring dynamic properties over a wide strain range with a single specimen is difficult. Most studies limit determination of dynamic properties to 1 % strain, despite evidence from past earthquakes indicating strains can exceed 5 % [21,22].

Previous studies have primarily developed modulus reduction and damping curves either for small strains range or for large strains range, often relying on separate specimens from different investigations and extrapolation of data for unavailable range. Table 1 presents a summary of existing shear modulus curves developed from experimental data. These studies compile data from diverse sources, each employing different testing equipment, soil types, and strain ranges. Consequently, combining data from specimens with varying properties and strain ranges may introduce inaccuracies [23,24]. This study addresses these limitations by performing combined resonant column and cyclic triaxial tests on a single specimen, capturing a continuous shear modulus response across a wide strain range (beyond 1 % strain). Disturbed and undisturbed soil samples representing various soil types were tested under different relative densities and confining pressures. Based on these single-specimen tests, a new empirical model is proposed to accurately predict normalized shear modulus up to 10 % shear strain. This model enhances the reliability of seismic response analyses, improving the accuracy of soil-structure interaction assessments and the design of foundations and earth structures.

2. Material characteristics, geological composition and sample preparation

The soils used in this study were collected from various geological deposits using drilling, tube sampling, augering, and open excavation, yielding both disturbed and undisturbed samples. Undisturbed samples were extracted from boreholes at different depths using PVC tube samplers (30 cm long, 7 cm diameter). Brahmaputra sand (BS) and Manu River sand (MRS) were obtained from the Northeast, while Mumbai Sand (MS) was obtained through open-pit excavation situated on the west coast of Peninsular India. Kalpakkam sand (KS) is retrieved from Kalpakkam Beach on the east coast of Peninsular India, and White sand (WS) is artificially crushed in Bangalore (South India). Furthermore, natural soil samples, designated as IGP1 to IGP4, were procured from the Indo-Gangetic Plains. An additional twenty-five samples were extracted from Uttar Pradesh, Northern India, at depths ranging from 5 m to 70 m, corresponding to effective confining pressures of 60 kPa, 200 kPa, 480 kPa, and 760 kPa. Sands from the United Kingdom were also tested under various relative densities and confining pressures.

The geological composition of these soil samples varies significantly due to their diverse origins. The Indo-Gangetic Plains are characterized by substantial Quaternary alluvial deposits, primarily comprising clay, silt, and sand, formed by the extensive fluvial activity of the Ganges and its tributaries. Coastal sands, such as those from Kalpakkam and Mumbai, are predominantly composed of quartz and feldspar minerals, typical of beach and dune sands. Sands from the Northeast, specifically Brahmaputra and Manu River sands, originate from the erosion of the Himalayan range, composed largely of sedimentary rocks like limestone and shale, alongside metamorphic rocks such as schist and gneiss. The artificially crushed sand from Bangalore is derived from the weathering of granitic rocks, which are prevalent in the region.

Table 1
Summary of shear modulus curves developed from experimental data.

Authors	Soil Type	Equipment	Number of Experiments/ Data	Range of shear strain (%) testing	Remarks
[14]	Sands, silty sands, gravels	*TC, SS, TS, CTX,*	Collected from different studies plus 75 tests	10^{-4} to 1	Proposed upper, lower, and mean curves for CP range of 28–400 kPa
[3]	Cohesionless	–	From literature	10^{-3} to 1	Curves proposed for PI ranging from 0 to 200
[25]	Gravely sand and gravel. Data from previous researchers are also taken.	*CTX and CTSS*	From literature	10^{-4} to 1	CP:50–450 kPa
[11]	Soils with PI ranging from 0 to 132	RC and TS	122	10^{-4} to 1	Depth: 0–326 m
[26]	Sand mica mixture	RC		10^{-3} to 10^{-1}	CP: 50–150 kPa
[16]	Quartz sand	Resonant Column Test	280	5×10^{-7} to 5×10^{-4}	CP:50–400 kPa
[27]	Sand/ Rubber, Gravel/ Rubber,	Resonant Column Test	126	2×10^{-4} to 0.3	CP:25–200 kPa
[28]	Pumice sand, Uniform quartz gravel	Resonant Column Test	30	5×10^{-4} to 10^{-3}	CP:25–400 kPa
[29]	Cohesionless	*RC, TS, SS, TSS, CTX*	454 from literature	10^{-4} to 10	CP: 50–600 kPa and a few tests below 50 kPa and above 600 kPa
[30]	Sand, clay and fiber soil composite	–	8 types of soils	10^{-3} to 10	Data was generated using DEEPSOIL software
[31]	Sand	CTX	9	1.5×10^{-3} to 3	CP: 50–150 kPa RD: 30–90 %
[32]	Cohesive soils	RC/Dam core	17 UD and14 RS	10^{-4} to 0.1	CP: 50–400 kPa

Abbreviations: RS: Remoulded samples, CP: confining pressure, CTX: cyclic triaxial test, RC: resonant column, TS: torsional shear, CTSS: cyclic torsional simple shear, SS: simple shear, TC: triaxial compression.

Index properties were determined according to ASTM standards, with specific gravities (G_S) ranging from 2.43 to 2.78. Grain Size Distribution (shown in Fig. 1) was analyzed via sieve and hydrometer methods [33]. Water content and bulk density were measured according to Refs. [34,35]. Plasticity limits were assessed per [36], while maximum and minimum densities were determined using the vibratory

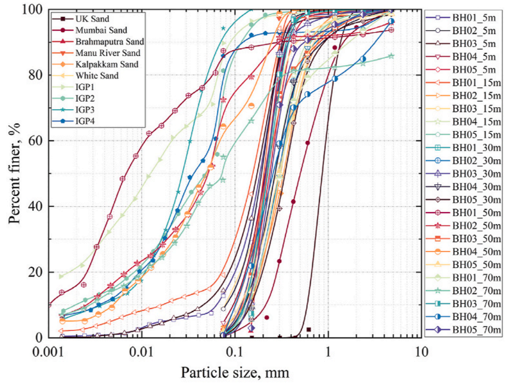

Fig. 1. Grain size distribution of soils used in the present study.

table method [37] and an alternative method for fine content exceeding 15 % [38]. Soil classification ranged from medium plasticity cohesive soils (plasticity index 10–20) to poorly graded sands. Fine content varied from 0 % to 94 %, and plasticity index from 0 to 15. The mean grain diameter ranged from 0.012 mm to 0.32 mm, and the coefficient of uniformity (C_U) varied from 0.83 to 38.46. Soils were categorized into cohesionless sands (fine content <5 %) and silty or clayey sands (fine content >5 % but plasticity index <15 %). Tables 1–4 summarize the physical properties of the soils used in this study.

For sample preparation, undisturbed samples were extruded to a specimen diameter of 5.4 cm and height of 10.5 cm using a sample extruder. Disturbed samples (BS, MRS, MS, UK, KS, WS) were reconstituted using dry tamping method at three relative densities (30 %, 60 %, 80 %) and tested under three confining pressures (50 kPa, 100 kPa, 200 kPa). Details on sample preparation methods are described in Refs. [39,40]. Combined resonant column and cyclic triaxial tests were then performed on the same specimen, in accordance with ASTM standards (D4015-21 and D5311-11). Resonant column testing was conducted to measure shear modulus at strain levels ranging from 0.0001 % to 0.05 %, while cyclic triaxial testing was conducted within a strain range of 0.05 %–10 %.

3. Test apparatus and testing procedures

To evaluate the shear modulus of various soils over a wide range of strains (0.0001 %–10 %), a combined resonant column and cyclic triaxial (RC-CTX) apparatus from Geotechnical Consulting and Test Systems (GCTS) was employed. The equipment was modified, calibrated, and validated post-modification to enable torsional resonant columns and cyclic axial loadings on the same specimen while maintaining sample integrity. The sample can be tested in both resonant column mode and cyclic triaxial mode, covering a strain range from 5×10^{-5} to ≥ 5 %. Fig. 2 shows the RC-CTX setup and its components. The resonant column test was used to determine the shear modulus for a shear strain range of 0.0001 %–0.05 %, while the cyclic triaxial test was used to calculate dynamic properties for strains of 0.05 %–10 %. The results from both tests were then combined to obtain dynamic soil properties over a wide strain range (0.0001 %–10 %).

The resonant column used for the present study is a fixed-free type where the torsional loading is applied at the top of the sample. Initially, the sample is tested in resonant column mode by applying a small confining pressure of 15 kPa and gradually increasing it to the desired effective confining pressure. Torsional loading is applied incrementally to determine the resonant frequency and shear wave velocity, from which shear modulus is calculated.

Torsional loading is applied in percentage full scale (*pfs*), corresponding to the maximum torque capacity of the resonant column's motor. A frequency sweep operation at a constant torque amplitude identifies the resonant frequency, with each sample undergoing 500 to 1000 cycles and an increment of 1 Hz. The resonant frequency is the frequency where maximum strain amplitude is observed. The 1 Hz increment was chosen to ensure a precise and efficient identification of the fundamental resonance peak while minimizing potential errors in shear wave velocity estimation. It also provides an optimal balance between measurement resolution and test duration, allowing accurate capture of the resonant frequency without excessive computational or experimental complexity. This step size is commonly used in resonant column testing [20,40] due to its effectiveness in achieving accurate results. A very low torque amplitude (e.g.,0.01 *pfs*) is selected initially as an input for the frequency sweep operation, followed by the subsequent increase of the torque amplitudes with each test (e.g., 0.1, 0.03, 0.05, 0.08, 0.1, 0.3, 0.6, 1, 2.5, 5, 8, 10, 15, 20 *pfs*). The shear wave velocity is obtained at each torque amplitude by measuring the first-mode resonant frequency using the equation (Eq (1)).

$$\frac{I}{I_o} = \frac{\omega h}{V_S} \tan\left(\frac{\omega h}{V_S}\right) \tag{1}$$

where, I is the mass moment of inertia of soil column $\left(I = \frac{md^2}{8}\right)$, m is the total mass of the soil sample, d is the diameter of the soil sample, I_o is the mass moment of inertia of the drive system including the top cap or added mass, V_S is shear wave velocity through the soil sample, ω is the natural circular frequency of soil sample, and h is the height of the soil sample. Once V_S is obtained, the shear modulus (G) can be calculated using $G = \rho\, V_S{}^2$.

After completing the resonant column test, the cyclic triaxial test is performed on the same sample by removing the cell pressure and applying a vacuum pressure of 15 kPa. The torsional motor is removed, and a piston rod is attached to the top of the sample, which is then re-enclosed in the chamber. The same cell pressure is reapplied to replicate the effective stress conditions of the resonant column test. The cyclic triaxial test is conducted in a stepped loading fashion, where constant axial strain amplitudes are applied through an actuator at the sample's top. Ten cycles of constant axial strain amplitude are applied at each loading step. Axial strains are measured using an axial proximeter, and axial deviatoric stress is measured using a load transducer. The resulting stress-strain graphs display hysteresis behavior.

Shear modulus (G) and shear strains (γ) are computed from Young's modulus (E) and axial strain (ε_a) using Equation (2). Double amplitude axial displacements are applied in steps of 0.04 mm, 0.07 mm, 0.09 mm, 0.15 mm, 0.30 mm, 0.45 mm, 0.60 mm, 0.75 mm, 0.90 mm, 1.50 mm,

Table 2
Physical properties of sands used in the present study: specific gravity (G_S), gravel content (G_C), sand content (S_C), fine content (F_C), coefficient of uniformity (C_U), coefficient of curvature (C_C), mean grain size (D_{50}), maximum and minimum void ratio (e_{max} and e_{min}).

Sample ID	G_S	G_C	S_C	F_C	C_U	C_C	D_{50}	e_{max}	e_{min}
BS	2.64	0.00	100.00	0.00	1.50	0.90	0.23	0.89	0.57
MRS	2.64	0.00	100.00	0.00	1.35	0.92	0.22	0.98	0.57
MS	2.67	0.85	98.96	0.00	2.54	0.79	0.51	0.67	0.44
WS	2.66	0.00	91.00	9.00	3.75	1.07	0.53	1.08	0.53
KS	2.56	0.00	96.60	3.40	2.56	1.03	0.34	0.92	0.55
UKS	2.65	0.00	100.00	0.00	1.37	0.92	0.90	0.71	0.50

Table 3
Physical properties of Indo-Gangetic Plains (IGP) soils: specific gravity (G_S), gravel content (G_C), sand content (S_C), fine content (F_C), coefficient of uniformity (C_U), coefficient of curvature (C_C), mean grain size (D_{50}), liquid limit (LL), plastic limit (PL) and plasticity index (PI).

Sample ID	G_S	G_C	S_C	F_C	Silt	Clay	C_U	C_C	D_{50}	LL	PL	PI	ISSCS
IGP1	2.70	0.00	12.09	87.91	66.91	21.00	8.68	1.79	0.0124	29.65	17.60	12.05	CL
IGP2	2.60	0.00	18.67	81.33	71.33	10.00	34.21	2.34	0.0489	29.56	20.48	9.08	CL
IGP3	2.56	0.00	5.75	94.25	87.25	7.00	8.68	1.79	0.0277	31.20	21.70	9.50	MI
IGP4	2.69	0.00	10.28	89.72	81.72	8.00	18.24	1.47	0.0358	33.23	29.18	4.06	ML

3.0 mm, 4.50 mm, and 6.00 mm. The shear modulus is calculated at each loading step, providing a variation of the shear modulus across a wide range of strains. Ten cycles of constant axial strain amplitude are applied at each loading step.

Fig. 3 illustrates typical results from the cyclic triaxial test on Manu river sand at a relative density of 60 % and a confining pressure of 50 kPa. Fig. 3a shows the stepwise loading of shear strain amplitude at different intervals. The legends indicate double amplitude axial strain. Fig. 3b plots the applied constant shear strain amplitude (0.9 %) against the number of cycles, and Fig. 3c presents the corresponding stress-strain plot, exhibiting the observed hysteretic behavior.

4. Estimation of shear modulus (G)

4.1. Evaluation of dynamic properties in resonant column apparatus

In the fixed free RC apparatus, a cylindrical soil specimen is placed on the rigid base and restrained at the bottom. Cyclic torsional loads are applied at the top through an electromagnetic drive system. The top of the specimen is restrained in the horizontal direction to prevent the development of any bending stresses in the soil column. A harmonic torsional load is applied, and the frequency of input loading is gradually varied (frequency sweep) in 1 Hz steps until the resonant frequency is identified. Resonant frequency corresponds to the maximum strain amplitude achieved during the frequency sweep. The shear wave velocity is subsequently calculated from the first mode of resonant frequency (Eq (1)), allowing for the determination of shear modulus $(G = \rho\, V_S^2)$

4.2. Evaluation of dynamic properties in cyclic triaxial apparatus

In this study, strain-controlled cyclic triaxial (CTX) tests were conducted to determine dynamic properties for a strain range of 0.05 %–10 % at a loading frequency of 1 Hz. Fig. 4 shows hysteresis loops obtained for MRS confined at an effective stress of 100 kPa and tested at a relative density of 30 %. The hysteresis loop exhibits symmetry at small strains; however, as shear strains increase, it becomes increasingly asymmetrical. This asymmetry at higher strain levels (in Fig. 3c and 4) arises due to the nonlinear behavior of soil under cyclic loading. At small to medium strains, the soil response remains elastic or quasi-elastic, maintaining symmetrical hysteresis loops. However, at large strain levels, fabric degradation, inter-particle slippage, and energy dissipation become significant, leading to asymmetry. The degree of asymmetry increases with increasing shear strain. In dry soil conditions, progressive stiffness degradation and strain localization further amplify this asymmetry.

Fig. 5a illustrates a schematic diagram of a hysteresis loop used in most of the previous studies by Refs. [14,20,41–43]. At small strains, the hysteresis loop is symmetrical, with the elastic modulus calculated from the slope of the line joining the origin to the peak compressive stress [14, 20]. However, as observed in this study and corroborated by Refs. [31, 44] the hysteresis loop becomes asymmetrical at large strains, making it difficult to define the shear modulus of soils. Fig. 5b shows a schematic diagram of the asymmetrical hysteresis loop along with different moduli calculations. Here, E_1 is defined as the slope from the origin to the maximum compressive stress, while E'_1 represents the slope to the maximum tensile (extension) stress. E_2 is the average of E_1 and E'_1, while E_3 is the slope connecting maximum tensile and compressive stresses. For a strain-controlled test, E_2 is theoretically equivalent to E_3, because strains developed during the compressive part of loading are the same as strains developed during the tensile part of loading. In the case of a symmetrical hysteresis loop, E_1, E_2, and E_3 are the same. The shear modulus (G) and shear strains (γ) are calculated from elastic modulus (E) and axial strains (ε_a) using Eq (2).

$$G = \frac{E}{2\,(1+\mu)\varepsilon_a} \text{ and } \gamma = (1+\mu)\varepsilon_a \tag{2}$$

where μ is Poisson's ratio and is typically set to 0.5 for undrained tests.

The shear moduli calculated using E_1, E'_1, E_2, and E_3 are referred to as G_1, G'_1, G_2, and G_3, respectively. In previous studies [44], utilized G_1, whereas [31] employed G_2 to calculate the shear modulus, without specifying which modulus is more suitable for soil shear modulus calculations. Fig. 6 presents a comparative analysis of different shear moduli, displaying significant deviations as shear strains increase. As shown in Fig. 6a, the moduli (G_1, G'_1, G_2, and G_3) are closely aligned at small strains, with minor deviations likely due to noise. However, at larger strains, the deviation among the moduli increases significantly, attributed to the asymmetric hysteresis response. G_1 exhibits higher values compared to G_2 and G_3, which remain similar due to the consistent development of tensile and compressive strains under strain-controlled conditions.

To quantify the deviation between G_1 and G_3 with respect to strains, the deviation is computed against G_1 for both MRS and KS, as shown in Fig. 6b. The plot indicates that at small strains, the deviation remains below 20 %, but escalates to approximately 130 % at larger strains. In the present study, G_2 (equivalent to G_3) is adopted as the shear modulus, as it accounts for the asymmetric hysteretic behaviour.

5. Results and discussions

This study investigates the effects of combined resonant column and cyclic triaxial tests (RC-CTX) on the same soil sample across a wide strain range (0.0001 %–10 %), aiming to minimize the effects of soil fabric changes during sample preparation. The RC-CTX test involves subjecting a soil specimen to resonant column vibrations, wherein the specimen undergoes numerous loading cycles at low strain levels during frequency sweeps, followed by cyclic triaxial loading. This process, involving torque application during RC and thousands of small strain cycles, may induce soil rearrangement potentially affecting test outcomes. To understand potential disturbances during resonant column testing, the soil samples used in combined RC-CTX testing were also subjected exclusively to cyclic triaxial vibrations at large strain amplitudes. These tests are termed cyclic triaxial tests only (CTXonly), while combined resonant column and cyclic triaxial results at large strain are termed CTXcombined for brevity.

Samples of Manu River sand, Kalpakkam sand, and Brahmaputra sand were reconstituted at various relative densities and subjected to three confining pressures (50, 100, 200 kPa), Both CTXcombined and CTXonly tests were performed. Fig. 7 shows the typical results for shear modulus variation with strain for Manu River sand samples. It can be observed that the normalized modulus reduction curves obtained from CTXonly tests closely align with those from CTXcombined tests at all

Table 4

Physical properties of Uttar Pradesh soils (northern part of India): bulk density (ρ_b), water content (w), and dry density (ρ_d), specific gravity (G_S), void ratio (e), degree of saturation (S), coefficient of uniformity (C_U), coefficient of curvature (C_C), mean grain size (D_{50}), gravel content (G_C), sand content (S_C), fine content (F_C), liquid limit (LL), plastic limit (PL) and plasticity index (PI), Indian Standard Soil Classification System (ISSCS), non-plastic (NP), silty sand-clayey sand (SM-SC), poorly graded sand (SP), low plasticity clay (CL), poorly graded sand with silt (SP-SM), intermediate plasticity clay (CI).

Name	Depth (m)	ρ_b (g/cc)	w (%)	ρ_d (g/cc)	G_S	e	S (%)	C_U	C_C	D_{50}	G_C	S_C	F_C	Silt	Clay	LL	PL	PI	ISSCS
BH01	5	1.75	15	1.52	2.72	0.79	52	3.49	1.58	0.20	0.22	87	12.78	12.22	0.56	27	NP	5.11	SM-SC
BH01	15	2.06	21	1.70	2.66	0.56	99	12.00	3.50	0.17	0.73	80.15	19.13	17.12	2	26	NP	4.38	SM-SC
BH01	30	1.8	16	1.55	2.67	0.72	59.28	1.59	0.96	0.23	0	99.75	0.25	N/A	N/A	36	NP	–	SP
BH01	50	1.78	36	1.31	2.71	1.07	91.13	10.84	1.18	0.01	6.25	6.35	87.4	72.15	15.25	48	22	26	CI
BH01	70	2.06	18	1.75	2.66	0.52	91.43	2.25	0.94	0.31	0.38	98.8	0.83	N/A	N/A	28	NP	–	SP
BH02	5	1.76	15	1.53	2.66	0.74	54	2.80	1.47	0.21	0	91.25	8.75	NA	NA	30	NP	7.3	SP-SM
BH02	15	1.57	15	1.37	2.68	0.96	42	2.13	0.98	0.32	0.02	98.85	1.12	N/A	N/A	37	NP	–	SP
BH02	30	2	19	1.68	2.70	0.61	84.58	2.15	0.96	0.30	0.1	98.7	1.2	N/A	N/A	37	NP	–	SP
BH02	50	2.13	17	1.82	2.68	0.47	96.50	24.17	1.81	0.05	3.93	23.55	72.52	64.33	8.19	30	NP	7.3	CL
BH02	70	2.07	19	1.74	2.66	0.53	95.51	38.46	1.92	0.07	14.23	30.75	55.02	46.96	8.06	24	NP	2.92	CL
BH03	5	1.76	17	1.50	2.71	0.80	58	4.49	1.59	0.19	0.33	85.35	14.32	14.11	0.21	31	NP	8.03	SC
BH03	15	1.57	19	1.32	2.7	1.05	50	1.81	1.01	0.23	0.28	98.06	1.66	N/A	N/A	30	NP	–	SP
BH03	30	1.93	21	1.60	2.68	0.68	82.74	1.70	0.98	0.23	0.05	98.55	1.4	N/A	N/A	31	NP	–	SP
BH03	50	1.99	17	1.70	2.7	0.59	78.14	2.37	1.12	0.23	0	97.98	2.02	N/A	N/A	28	NP	–	SP
BH03	70	1.39	22	1.14	2.67	1.34	43.72	1.66	0.96	0.24	0.02	99.2	0.78	N/A	N/A	34	NP	–	SP
BH04	5	1.77	21	1.46	2.66	0.82	68	2.43	1.21	0.22	0	95.43	4.58	N/A	N/A	33	NP	–	SP
BH04	15	1.57	20	1.31	2.66	1.04	52	2.01	0.98	0.27	0.85	98.25	0.9	N/A	N/A	32	NP	–	SP
BH04	30	1.82	6	1.72	2.70	0.57	28.30	2.02	0.96	0.27	0.18	98.58	1.25	N/A	N/A	29	NP	–	SP
BH04	50	2.05	18	1.74	2.66	0.53	90.15	13.36	1.45	0.05	0	35.68	64.33	59.24	5.09	32	NP	8.76	CL-ML
BH04	70	1.96	15	1.70	2.66	0.56	71.16	2.87	1.00	0.26	3.58	95.63	0.8	N/A	N/A	25	NP	–	SP
BH05	5	1.63	17	1.39	2.71	0.95	49	1.77	0.97	0.25	0	99.55	0.45	N/A	N/A	35	NP	–	SP
BH05	15	1.6	15	1.39	2.69	0.94	44	2.11	0.95	0.30	0.3	99.55	0.15	N/A	N/A	31	NP	–	SP
BH05	30	1.6	10	1.45	2.70	0.86	31.53	2.36	0.96	0.35	1.47	97.88	0.65	N/A	N/A	30	NP	–	SP
BH05	50	1.62	36	1.19	2.75	1.31	75.65	2.87	1.05	0.30	1.35	96.7	1.95	N/A	N/A	28	NP	–	SP
BH05	70	1.88	20	1.57	2.66	0.70	76.23	1.67	0.96	0.25	0.07	99.23	0.7	N/A	N/A	33	NP	–	SP

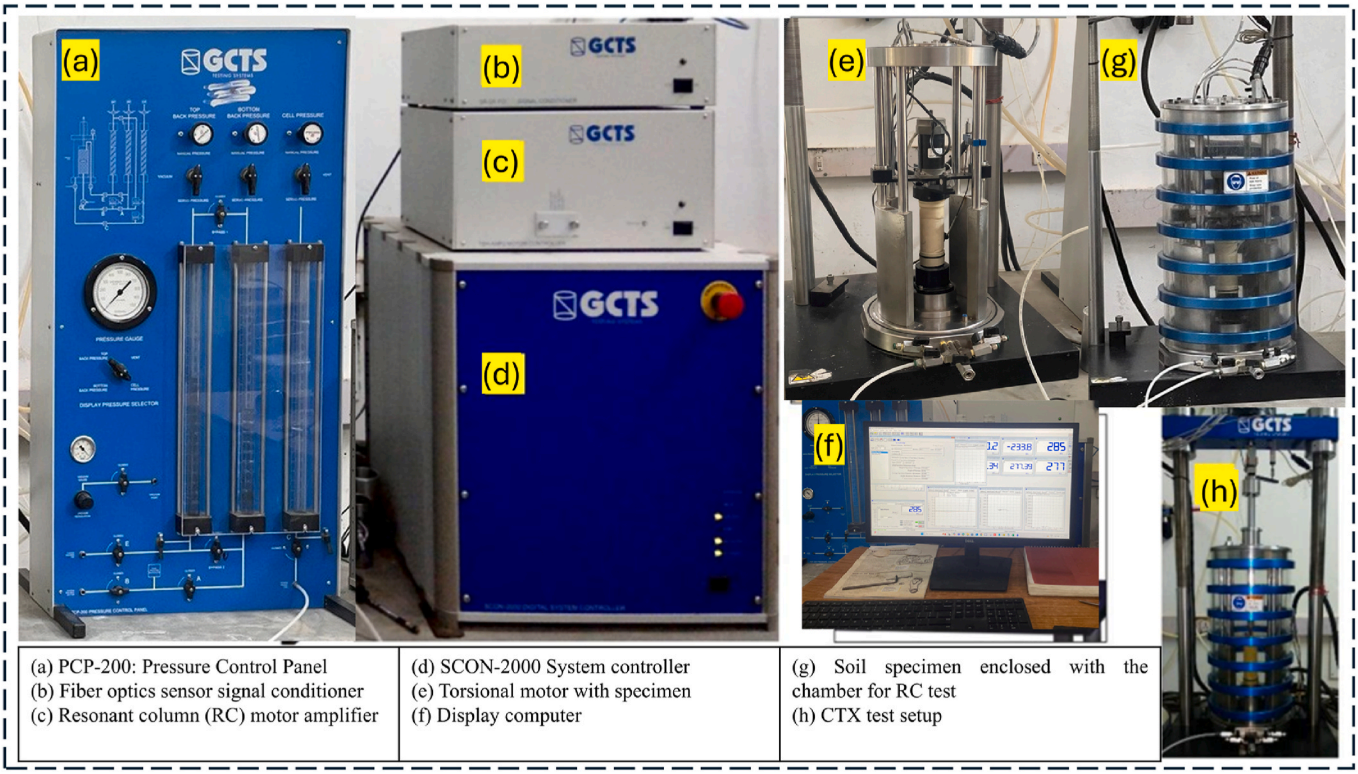

Fig. 2. Combined resonant column and cyclic triaxial setup and its components.

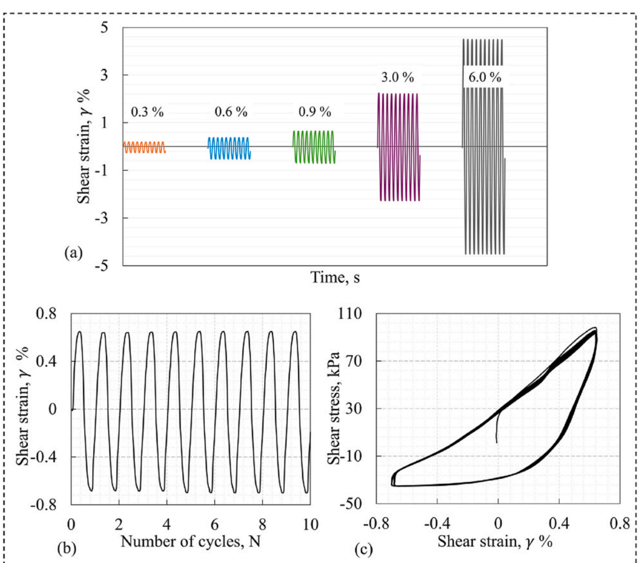

Fig. 3. Typical plots from the cyclic triaxial test on Manu river sand (relative density of 60 %, confining pressure 50 kPa) (a) stepped loading at different shear strain amplitudes, (b) shear strain versus number of cycles, and (c) shear stress versus shear strain for ten loading cycles.

three confining pressures. A slight deviation observed at the start of the test is attributed to vacuum left inside the soil samples when mode of loading is changed. Similar results were observed for Kalpakkam sand and Brahmaputra sand samples. These findings confirm that disturbances during resonant column testing are insignificant and do not significantly influence the shear modulus in combined RC-CTX testing. The negligible differences in shear modulus between CTXcombined and CTXonly, as observed in all tested sands, support the reliability of using a single specimen for both RC and CTX testing. This approach not only minimizes time for sample preparation and testing but also ensures consistency in results. Further details, including the minimal influence of prior strain history on shear modulus, are provided in Ref. [45]. Consequently, combined RC-CTX tests were conducted on additional soil samples from diverse regions, and the results are discussed herein. It can be noted that variations in G due to sample preparation are not studied here.

5.1. Influence of relative density and confining pressure

To understand the effect of relative density and confining pressure on the stiffness of soils over a wide strain range, combined RC-CTX tests were conducted on various clean sand samples, including Brahmaputra sand (BS), Manu River sand (MRS), Mumbai sand (MS), Kalpakkam sand (KS), and Bangalore/White sand (WS). Table 2 provides the physical properties and soil classification; the majority of soils were classified as poorly graded sands (SP).

Fig. 8 shows the modulus reduction curves obtained for Brahmaputra sand (Fig. 8a), Mumbai sand (Fig. 8b), Manu River sand (Fig. 8c), and Kalpakkam sand (Fig. 8d). The nomenclature used in the symbols is RD_CP, where RD represents relative density and CP represents confining pressure. It can be observed that for all the sands, at a given relative density and confining pressure, as the shear strains increase, the shear modulus decreases continuously. The reduction in shear modulus is less pronounced in the small strain range than in the large strain range. The shear modulus remains constant in a small strain range; in other words, soil behaves elastically for shear strains less than 10^{-2} %. The strain amplitude up to which shear modulus remains constant is called elastic threshold strain (γ_e). Beyond γ_e, shear modulus decreases, and soil starts behaving non-linearly. The shear modulus at this strain range is called small strain shear modulus or maximum shear modulus (G_{max}). A slight increase in the modulus values was observed for some samples at a strain level of 0.05 %, where the mode of loading is changed. The slight jump in the modulus values can be due to the residual vacuum pressure left inside the sample. A residual vacuum is the

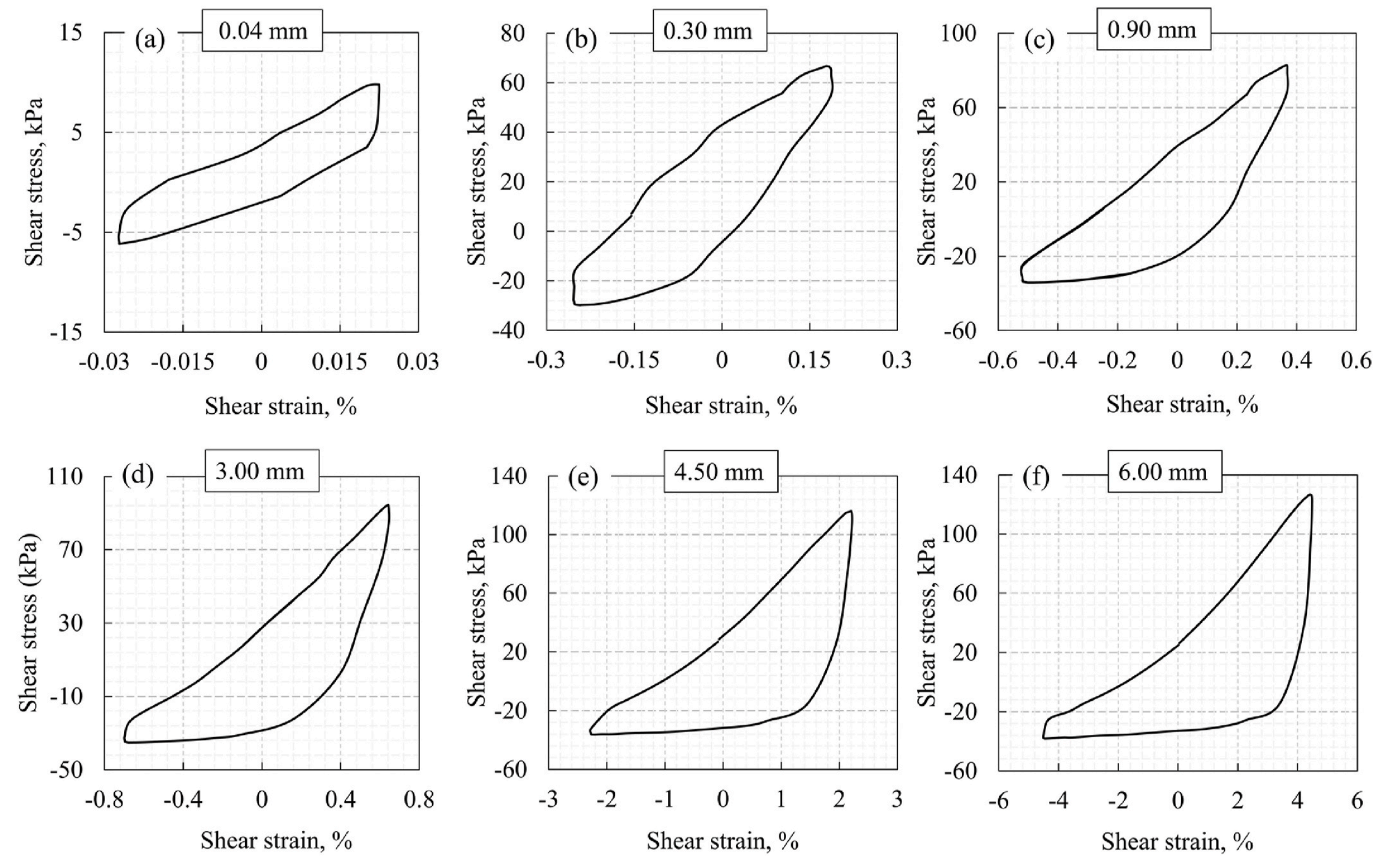

Fig. 4. Stress-Strain hysteresis loops at axial deformation of (a) 0.04 mm, (b) 0.30 mm, (c) 0.90 mm, (d) 3.00 mm, (e) 4.50 mm, and (f) 6.00 mm.

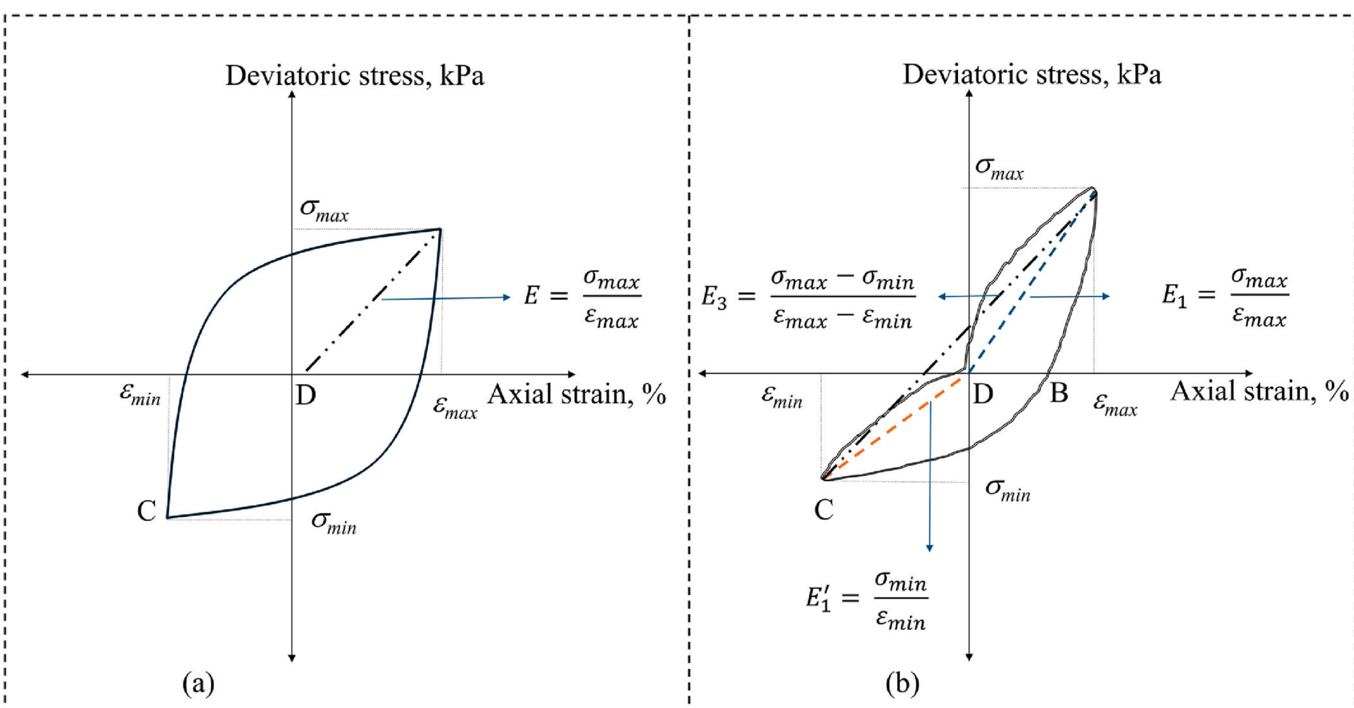

Fig. 5. (a) Symmetric hysteresis loop at small strains, and (b) asymmetrical hysteresis loop at large strain.

vacuum pressure that remains inside the sample after releasing the vacuum inside the sample. It can also be observed from Fig. 8 that in all the samples at a given shear strain and relative density, shear modulus increases as the confining pressure increases. With the increase in confining pressure, void spaces between the sand grains tend to decrease, resulting in an increase in particle-particle contact forces and

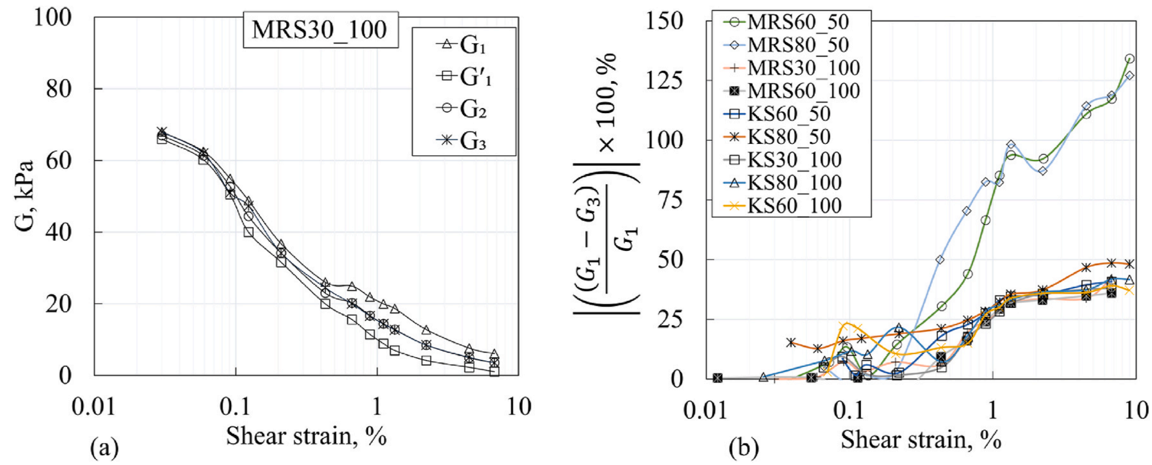

Fig. 6. (a) Comparison of different shear moduli of MRS prepared at 30 % relative density and tested at 100 kPa effective confining stress at different strains, (b) Deviation between G_1 and G_3 computed for MRS and KS at different relative densities and effective stresses.

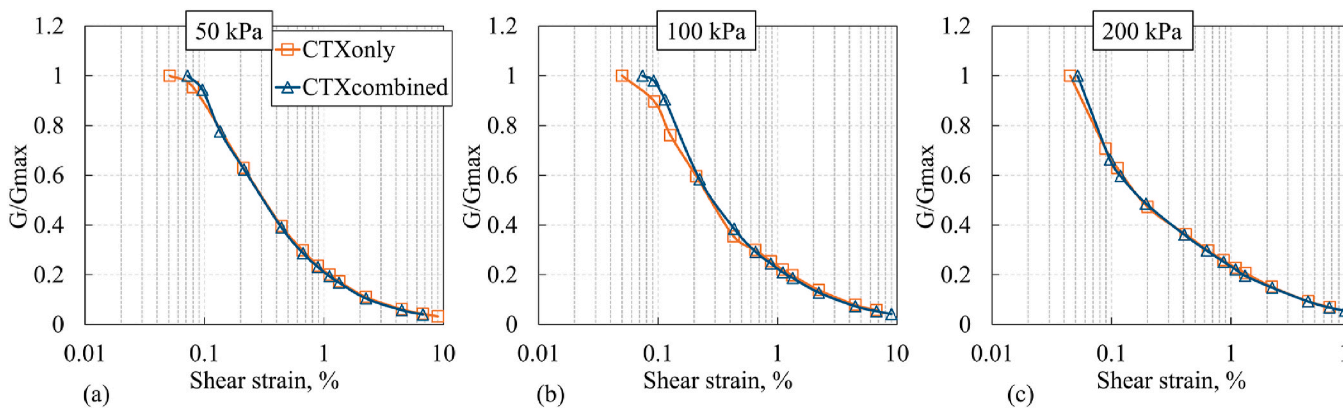

Fig. 7. Comparison of normalized modulus reduction curves between cyclic triaxial tests (CTXonly) and combined resonant column-cyclic triaxial tests (CTXcombined) at 60 % relative density for effective confining pressure of (a) 50 kPa, (b) 100 kPa, and (c) 200 kPa, respectively.

better arrangement of particles, which in turn leads to increased stiffness. Similar findings were reported by [1,2,11,14,20,46].

At a given shear strain level and confining pressure, an increase in shear modulus is observed as the relative density increases (Fig. 8). At higher density, the larger number of particles in a given volume causes greater resistance to deformation and rearrangement of soil particles, leading to higher stiffness. At large strains (>0.5 %), the shear modulus values tend to converge, indicating that the effect of relative density and confining pressure is more pronounced at small to medium strains. At very large strains (1 %–10 %), samples tested at the same confining pressure tend to align closely, implying that the shear modulus is independent of relative density at large strains (nested figs. In Fig. 8c and d). For samples reconstituted at the same relative density, the curves obtained at different confining pressures display a clear and consistent trend. This observation of the lesser effect of relative density on modulus reduction curves was also made by Refs. [31,46,47] for gravels. Due to the rearrangement of soil particles, loose states become denser, and dense states become slightly looser, leading to converging curves at large strains.

To minimize the effect of confining pressure and facilitate comparison of results across different materials and model calibrations, the modulus reduction curve is normalized by the maximum shear modulus (G_{max}). Fig. 9 presents the normalized modulus reduction curves for Brahmaputra sand. Upon normalization with G_{max}, the curves closely tend to align. At a constant relative density, increasing confining pressure shifts the normalized reduction curve to the right for all three relative densities (Fig. 9a, b, and c), indicating reduced nonlinearity with higher confining pressure. This observation is consistent with findings by Refs. [1,48,49]. Further, the effect of confining pressure is more pronounced at lower relative densities and diminishes as the relative density increases, causing the curves to converge. Additionally, the influence of confining pressure on the normalized modulus reduction rate is more noticeable at large strains and less significant at smaller strains. Fig. 9d, e, and f illustrate the effect of relative density while keeping confining pressure constant. Regardless of the confining pressure, the curves remain close to each other, suggesting that relative density has a minimal effect on the normalized reduction curve. This finding concords with observations by Refs. [1,47]. Similar trends in modulus reduction and normalized modulus reduction curves were observed for all samples tested in the study, though these results are not presented here for brevity.

5.2. Comparison of data with previous literature

Disturbed and undisturbed samples were collected from different depths and locations across India to study variability in soil properties and confining pressures. The effective confining pressure in the present study ranges from 60 kPa to 1000 kPa. The shear modulus data was analyzed and compared with available curves and models in the literature. Fig. 10 compares modulus reduction data of soils used in the present study with the mean, upper, and lower bounds curves proposed by Refs. [3,14] for plasticity index (PI) of 0, and [50] at an effective

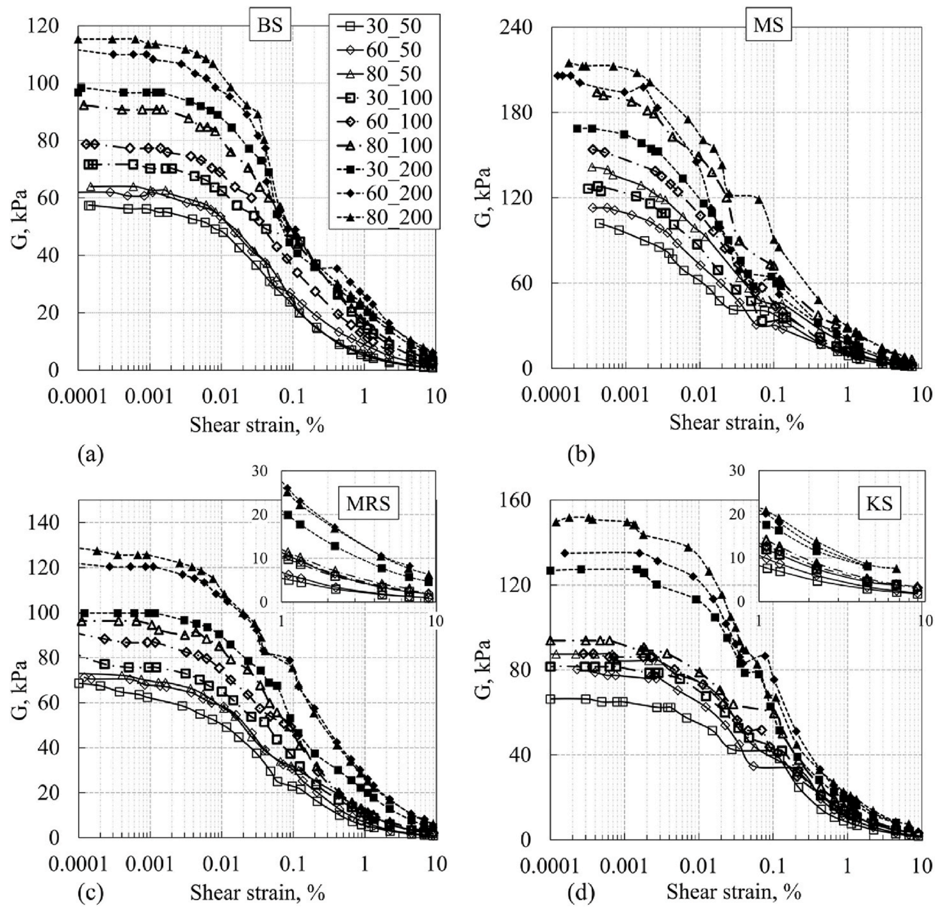

Fig. 8. Shear modulus reduction curve for Brahmaputra sand (BS), Mumbai sand (MS), Manu river sand (MRS), and Kalpakkam sand (KS).

confining stress of 95.76 kPa and 957.61 kPa. These curves are most commonly used in geotechnical engineering practice for seismic response analysis for sites predominantly with sand fraction.

The Vucetic and Dobry curve [3] at PI of 0 aligns closely with the mean Seed and Idriss curve [14], while the EPRI curve [50] at 95.76 kPa aligns with the upper bound Seed and Idriss curve [14]. Fig. 10a and b shows the comparison of soils with $F_C < 5$ % and soils with $F_C > 5$ %, respectively. A significant scatter and deviation from these established curves were observed, possibly due to the lower confining pressures and narrower strain ranges considered in previous studies (Table 1). From Fig. 10a, it can be noticed that at small strains (<0.01 %), the normalized shear modulus data both fall below and exceeds the Seed and Idriss curves. As strains increase, the data aligns more closely with the upper bound and exceeds it beyond a shear strain of 0.2 %. For strains less than 0.1 %, the normalized shear modulus reduction data falls below the EPRI curve at 957.61 kPa but exceeds it at higher strains.

Fig. 10b displays modulus reduction curves for soils with fine content greater than 5 % and a plasticity index ranging from 0 to 15 %. It is observed that the modulus reduction data lies below the Vucetic and Dobry curve at a PI of 30 and EPRI curve at 957.61 kPa. However, beyond 0.2 % strain, EPRI curve displays an abrupt drop in stiffness compared to Vucetic and Dobry curves [3]. The mean curve of Seed and Idriss align with the observed modulus reduction data up to 0.01 % strain but falls below beyond this point. At larger strains (>1 %), the data converge closely, suggesting that fine content and plasticity index have minimal influence on large strain shear modulus. This behavior is attributed to finer particles moving into void spaces and the breaking of plastic bonds at large strains. The 5 % fine content cutoff is based on observed shifts in modulus reduction trends from the experimental data, which aligns with previous studies [46]. For FC < 5 %, fines act as void fillers with minimal impact on stiffness, resembling clean sand behavior. Beyond 5 %, fines influence plasticity, and cohesion, altering soil response. This 5 % threshold provides a practical classification for analyzing soil behavior variations, especially in the complex geology of the Himalayan region, and aids in assessing site-specific earthquake ground motion hazards. It can be concluded that none of the curves accurately predict shear modulus for strains up to 10 %. Seed and Idriss [14] and Vucetic and Dobry predict mean shear modulus values up to 0.02 % strain, while EPRI curve at 95.76 kPa overestimates shear modulus for both soil categories. EPRI curve at 957.61 kPa closely predicts shear modulus up to 0.1 % strain but underestimates it significantly beyond this point. Comparing Fig. 10a and b, it is evident that soils with fine content >5 % exhibit less deviation compared to soils with fine content <5 %.

To investigate soil behavior under large confining pressures, samples were extracted from five boreholes at depths of 50 m and 70 m. Fig. 11 presents the modulus reduction curves for soils from these boreholes (BH01, BH02, BH03, BH04, and BH05) at varying depths, corresponding to effective stresses of 760 kPa and 950 kPa, respectively. It can be noticed that despite the high confining pressures, significant scatter is observed in the modulus reduction curves. Although increased confining pressures (760 kPa and 950 kPa) reduce variability, modulus reduction remains influenced by intrinsic soil properties. This scatter is likely due to variations in fine content (up to 94 %), coefficient of uniformity (up to 38.46), mean grain size (0.012–0.32 mm), and water content (up to 36 %). At large strains, particle breakage, grain rearrangement, and induced anisotropy further contribute to this variability. Soils with high silt (up to 81.72 %) and clay (up to 21 %) exhibit different stiffness degradation, which is also influenced by plasticity (PI up to 15). Additionally, in-situ factors such as stress history and potential cementation

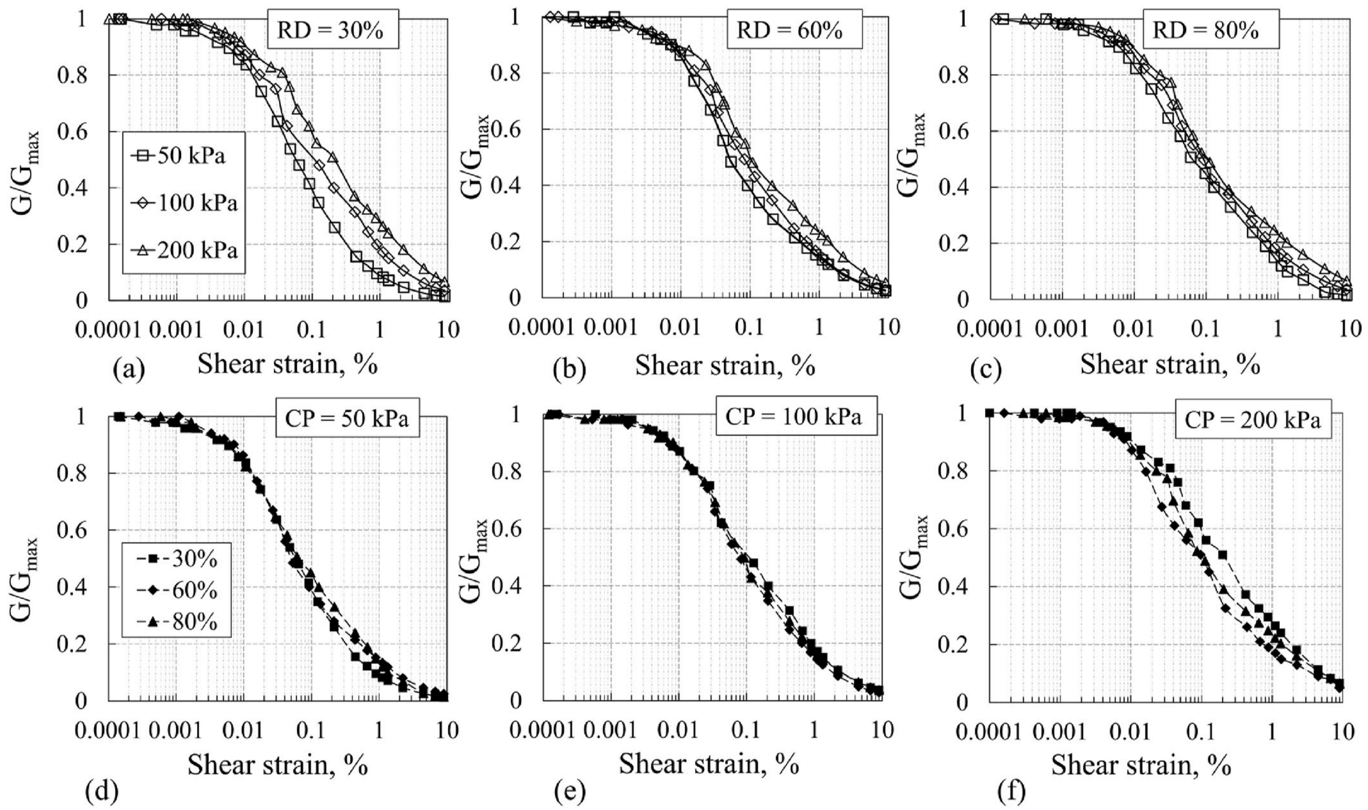

Fig. 9. (a)–(c) Effect of confining pressure on the modulus reduction at constant relative density. (d)–(f) Effect of relative density on the modulus reduction curve at constant confining pressure for Brahmaputra sand.

may affect modulus reduction. Further analysis is required to quantify these effects through statistical correlations and a detailed investigation into soil structure and fabric.

The data were compared with the mean curve of Seed and Idriss [14] and the EPRI curves [50] at 95.76 kPa and 957.61 kPa. At large strains, the normalized shear modulus data lie above the EPRI curve [50] developed at 957.61 kPa. Observations from Figs. 10 and 11 underscore the need for a new modulus reduction curve utilizing a combined loading system. Previous curves were primarily derived from data collected in different studies conducted globally, which were confined to a narrow strain range (Table 1). Moreover, these studies often combined low-strain test data from one sample with large-strain test data from another, leading to inaccurate and non-representative shear modulus estimations. Therefore, it is necessary to propose new sets of mean, upper, and lower bound curves to enable accurate seismic response analyses for Indian Himalayan region soils in the absence of direct experimentation.

5.3. Empirical relationships

Shear modulus is a key parameter in seismic response analysis, typically determined experimentally. To complement these methods, several researchers have proposed empirical models to estimate shear modulus as a function of shear strain, confining pressure, void ratio, coefficient of uniformity, and plasticity index. The hyperbolic model [20,51,52] describes nonlinear stress-strain behavior, where shear modulus decreases with increasing strain. It reaches a maximum value (G_{max}) at low strains and asymptotically approaches zero at higher strains. The original hyperbolic model is expressed as [20]:

$$\frac{G}{G_{\max}} = \frac{1}{1 + \frac{\gamma}{\gamma_{\text{ref}}}} \tag{3}$$

where γ_{ref} is reference strain, defined as $\gamma_{ref} = \frac{\tau_{max}}{G_{max}}$.

Due to the challenges in obtaining reference strain [2], later proposed a two-parameter modified hyperbolic model. In this model, the first parameter is the modified reference strain, which is defined as the shear strain corresponding to a 50 % reduction in shear modulus (i.e., $G/G_{max} = 0.5$). The second parameter is the Curvature coefficient (a), which influences the shape of the normalized shear modulus reduction curve. This modified hyperbolic model was subsequently adopted by Refs. [11,47,53], and is also implemented in seismic response analysis software. The model is expressed as:

$$\frac{G}{G_{\max}} = \frac{1}{1 + \left(\frac{\gamma}{\gamma_{\text{ref}}}\right)^{a}} \tag{4}$$

Higher values of γ_{ref} result in a rightwards shift in the curve, implying higher linearity or delayed nonlinearity. Oztoprak and Bolton model [29] proposed a further modification to Darendeli's hyperbolic model, introducing a three-parameter version as shown in Eq. (5). This model includes an additional parameter, known as the elastic threshold strain (γ_e), which is defined as the strain value at which the shear modulus remains constant and equal to maximum shear modulus.

$$\frac{G}{G_{\max}} = \frac{1}{1 + \left(\frac{\gamma - \gamma_e}{\gamma_{\text{ref}}}\right)^{a}} \tag{5}$$

For soils with plasticity [10], proposed an equation to compute the normalized shear modulus as a function of plasticity index (PI), as shown in Eq. (6).

$$\frac{G}{G_{\max}} = K(\gamma, PI)\ \sigma'^{(m(\gamma,PI) - m_o)} \tag{6}$$

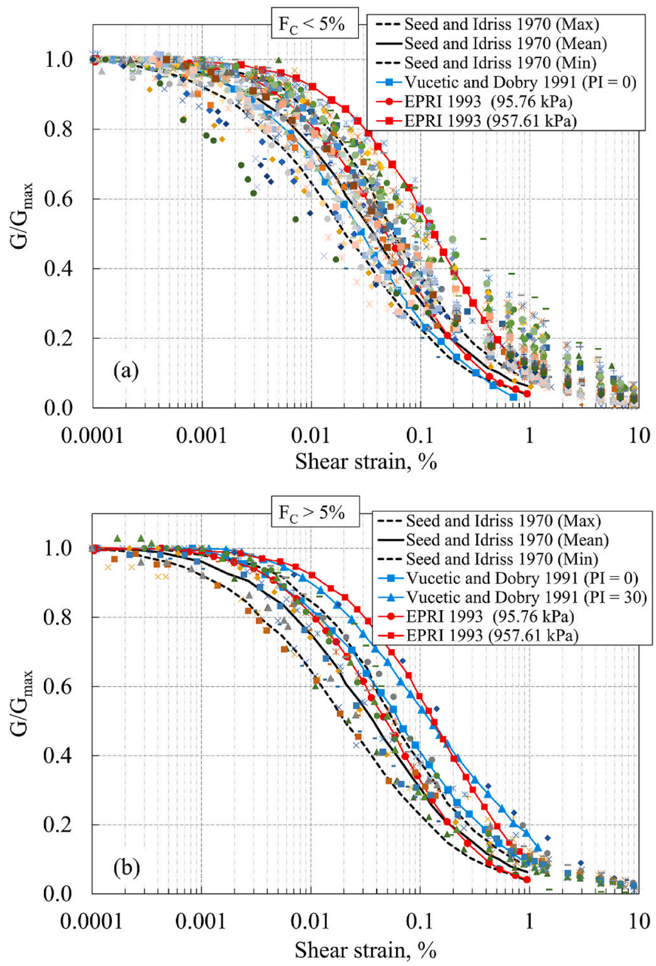

Fig. 10. Comparison of normalized shear modulus data for (a) sands (fine content <5 %) and (b) fine-rich soils (fine content >5 %) with established curves in the literature.

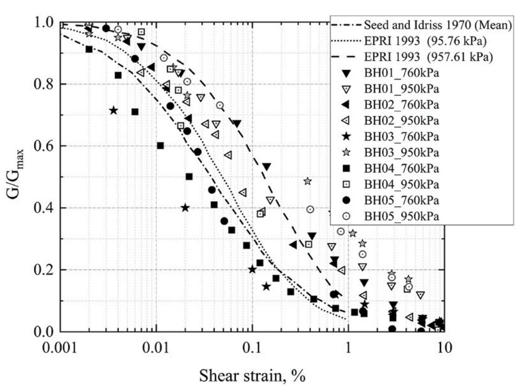

Fig. 11. Normalized modulus reduction at large confining pressures compared with mean Seed and Idriss (1970) and EPRI (1993) curves.

where, $m(\gamma, PI) - m_o = 0.272\left[1 - \tanh\left\{\ln\left(\frac{0.000556}{\gamma}\right)^{0.4}\right\}\right]e^{-0.0145PI^{1.3}}$

$$K(\gamma, PI) = 0.5\left[1 + \tanh\left\{\ln\left(\frac{0.000102 + n(PI)}{\gamma}\right)^{0.492}\right\}\right]$$

$$n(PI) = 0 \text{ for } PI = 0 \text{ and } \begin{matrix} 3.37\times10^{-6}PI^{1.404}; & 0 \le PI \le 15 \\ 7.0\times10^{-7}PI^{1.976}; & 15 \le PI \le 70 \\ 2.7\times10^{-5}PI^{1.115}; & PI > 70 \end{matrix}$$

Recently [30], proposed a universal model for predicting the shear modulus of sands, clays, and fiber-soil composite soils. A four-parameter model, as shown in Eq. (7), was developed to estimate the normalized modulus reduction curve as a function of shear strain (γ).

$$\frac{G}{G_{\max}} = {}^{1}\!/\!\left(1 + b_1\gamma^{b_2}\, \acute{e}\left(b_3\gamma + b_4\gamma^2\right)\right) \tag{7}$$

In the present study, the experimentally obtained shear modulus data were analyzed using the two-parameter (Eq. (4)), the three-parameter (Eq. (5)) and the four-parameter model (Eq. (7)) proposed by Refs. [2,29,30]. Model performance was evaluated through the coefficient of determination (R^2) and root mean square error (RMSE), with higher R^2 and lower RMSE indicating better accuracy. Fig. 12 compares the experimental normalized modulus reduction data with the curves obtained through nonlinear regression using these models. The results show that the models by Refs. [2,30] provide more accurate predictions than the Oztoprak and Bolton model, as evidenced by higher (R^2) values and lower RMSE. The Oztoprak and Bolton model shows reduced accuracy, likely due to its limitation in providing shear modulus values for strains below the elastic threshold strain (γ_e).

Fig. 13a shows the effect of confining pressures on the normalized modulus reduction curves for Manu River sand at 30 % relative density, tested under 50 kPa, 100 kPa, and 200 kPa confining pressures. Fig. 13b displays the effect of relative density on the sand 30 %, 60 %, and 80 % relative densities under 100 kPa confinement. Fig. 13a reveals that, with constant relative density, higher confining pressures shift the curves rightward, indicating a slower rate of shear modulus reduction with increasing confining pressure. Conversely, Fig. 13b demonstrates that the influence of relative density on shear modulus is less distinct. At large strains, both relative density and confining pressure effects diminish, as confirmed by experimental results. Nonlinear regression analysis was performed on each sample individually, using Darendeli's two-parameter hyperbolic model, and it showed R^2 values ranging from 0.936 to 0.999, indicating a strong fit to the experimental data.

Further, Fig. 13 reveals that as confining pressure increases, the reference strains shift to the right. This shift indicates that the onset of non-linearity in the soil's behavior is delayed with increasing confining pressure. For clean sands, the reference strain ranges from 0.008 % to

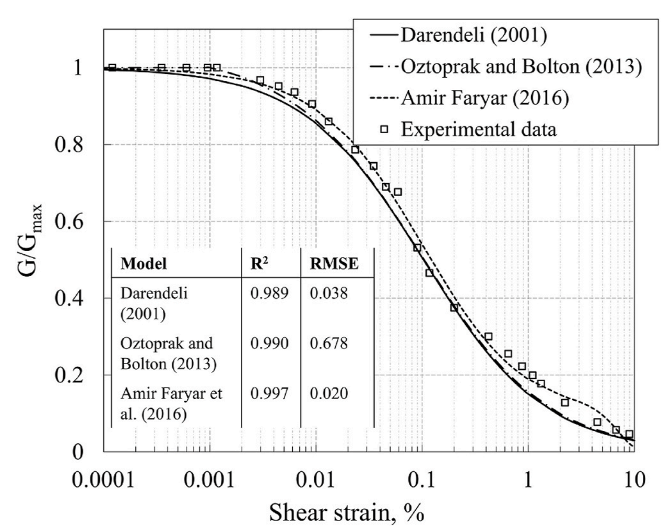

Fig. 12. Comparison of experimental normalized shear modulus data for Manu river sand at 30 % relative density and 100 kPa confining pressure with the models of Darendeli (2001), Oztoprak and Bolton (2013), and Amir Faryar et al. (2016).

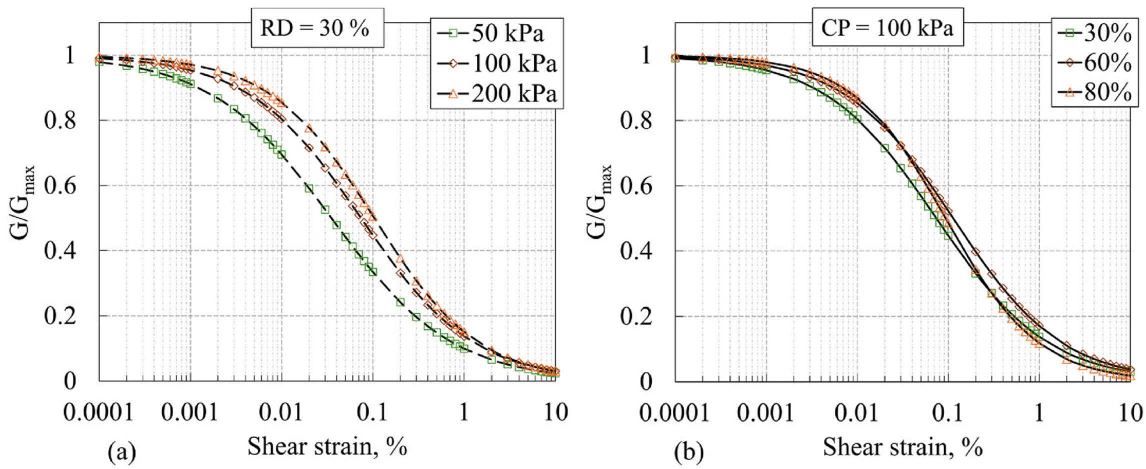

Fig. 13. Normalized shear modulus reduction curve for Manu River sand: (a) at various confining pressures and (b) at different relative densities, obtained from nonlinear regression analysis using the two-parameter model by Darendeli (2001).

0.4 %. Conversely, for soils with fines content greater than 5 %, the reference strain ranges from 0.02 % to 0.2 %. The narrower range observed in soils with higher fines content may be attributed to the influence of plasticity.

As previously discussed, Darendeli's model depends on two key parameters: reference strain and curvature coefficient. The effects of confining pressure, relative density, and the coefficient of curvature on these parameters have been investigated for BS, MRS, MS, UKS, and WS soils, with the resulting curves presented in Fig. 14. Fig. 14a demonstrates that as confining pressure increases, the reference strain also increases, while the curvature coefficient remains relatively constant for a given relative density. Conversely, with constant confining pressure, an increase in relative density leads to ambiguous trends in both reference strain and curvature coefficient, as shown in Fig. 14b. Fig. 14c

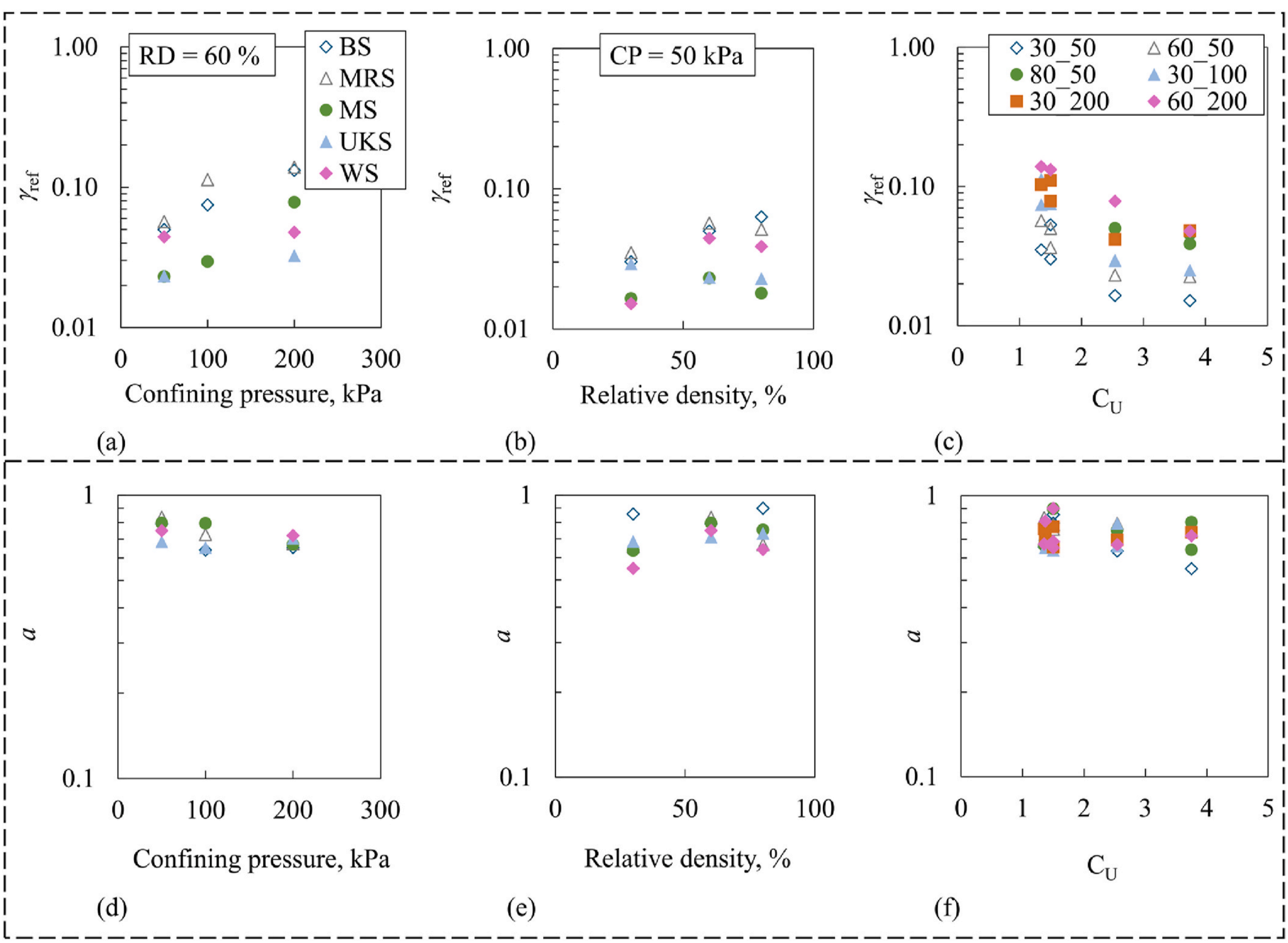

Fig. 14. Dependency of 'γ_{ref}' and parameter 'a' on (a, d) confining pressure, (b, e) relative density, and A(c, f) coefficient of uniformity (C_U).

indicates that as the coefficient of uniformity increases, the reference strain decreases, while the curvature coefficient remains nearly unchanged. The observed decrease in reference strain (γ_{ref}) with increase in C_U can be attributed to the effect of grain size distribution on soil stiffness and strain mobilization. As C_U increases, a wider grain size distribution allows smaller particles to fill voids between larger grains, enhancing particle contact density and restricting free grain rearrangement under shear loading. Additionally, higher C_U slightly reduces compressibility, further contributing to the decrease in reference strain. In contrast, the curvature coefficient 'a' remains nearly unchanged, as it is more influenced by particle shape, mineralogy, and inherent anisotropy rather than grain size distribution. Similar findings have been reported in studies on normalized modulus reduction behavior [13,16], where C_U was found to affect γ_{ref} more than the curvature parameter 'a'. The parameter 'a' range from 0.5 to 0.9, consistent with [13] findings that the values typically fall within the range of 0.5–1. Higher values of parameter 'a' imply gradual degradation of shear modulus with shear strain. Fig. 14d, e, and f, indicate that while parameter 'a' remains nearly constant and largely independent of confining pressure, relative density, and C_U, slight fluctuations in empirical fitting may arise due to variations in soil fabric, fines content, local void ratio differences and interparticle interactions. Additionally, nonlinearity in soil response at higher strains may introduce some scatter. However, the overall trend confirms the stability of 'a' across different conditions, supporting its intrinsic nature.

Several researchers have proposed various expressions to determine the reference strain, as summarized in Table 5. Using these expressions, the reference strain has been evaluated at different confining pressures and relative densities for soils with fines content both below and above 5 %. The analysis indicates a strong correlation between the reference strain, effective confining pressure, and coefficient of uniformity. For soils with fines content below 5 %, the R^2 and RMSE values are 0.83 and 0.70, respectively, while for soils with fines content above 5 %, the values are 0.82 and 0.036. The RMSE value of 0.70, reflects the inherent variability due to the large dataset, which includes both disturbed and undisturbed soil samples tested under various relative densities and confining pressures. While undisturbed samples retain their natural structure, reconstituted samples exhibit fabric variations, contributing to data scatter and higher RMSE values. Previous studies [2] have also reported similar levels of deviation in empirical models. Despite the RMSE value, the coefficient of determination ($R^2 = 0.83$) indicates a reasonably strong correlation, supporting the model's reliability. Fig. 15 presents a surface plot illustrating the relationship between reference strain, confining pressure, and coefficient of uniformity for both soil types. In both cases, the reference strain reaches its maximum at higher confining pressures and lower coefficients of uniformity.

Table 5
Models for reference strain (γ_{ref}) in the literature and proposed in the present study.

Model	Reference strain (γ_{ref})	Parameters
[54]	$a \times \left(\frac{\sigma}{P_a}\right)^b$	a = 0.0621, b = 0.5023
[13]	$a \times C_U^b \times \left(\frac{\sigma}{P_a}\right)^c$	a = 0.12, b = −0.6, c = $0.5 \times C_u^{-0.15}$
[28]	$a \times e^{b \times C_U} \times \left(\frac{\sigma}{P_a}\right)^c$	a = 0.159, b = −0.419, c = 0.42
[16]	$a \times e^{b \times \ln(C_U)} \left(\frac{\sigma}{P_a}\right)^c \times e^{d \times FC^e}$	a = 0.0652, b = −0.59, c = 0.4, d = 0.33, e = 0.1
[42]	$a \times C_U^b + c$	a = 14.08, b = −2.83, c = 0.129, $C_U < 15$
Present study	$a_1 \times \left(\frac{\sigma}{P_a}\right)^b \times C_U^c$	($F_C < 5$ %) $a_1 = 0.001 \times RD + 0.0575$, $b = -0.0015 \times RD + 0.8349$, c = −0.8720, ($F_C > 5$ %) $a_1 = 0.0327$, b = 0.8695, c = −0.2130,

P_a = Atmospheric pressure (100 kPa), σ = mean effective confining pressure.

A three-parameter power-law model, listed in Tables 6, is employed to describe the evolution of reference strain with confining pressure and coefficient of uniformity. Parameters 'a_1' and 'b' show a linear dependence on the relative density of clean sands ($F_C < 5$ %), while parameter c shows no significant trend. As shown in Fig. 16, 'a_1' increases while 'b' decreases with increasing relative density. A higher 'a_1' indicates a steeper drop in γ_{ref} with increasing C_U and decreasing CP, which implies that the highest drop is obtained at large confining pressures and small C_U values. A decreasing 'b' value suggests that the effect of confining pressure is less significant at higher relative densities.

Additionally, regression analysis using a two-parameter Darendeli model [Eq no 4] was performed on all the experimentally obtained shear modulus data for soils within each category. Table 6 lists the coefficients and parameters for soils with FC < 5 % and FC > 5 %. The mean values of parameter a and reference strain represent the average shear strains at which 50 % reduction in shear modulus occurs. The minimum and maximum parameters, corresponding to lower and upper bound curves, are derived from experimental data considering the extreme minimum and maximum of that particular category of soils. Fig. 17a and b shows the mean, upper and lower bounds proposed from the present study. These models can be applied directly in the absence of specific soil properties and depth information.

Fig. 18 plots the residuals for both soil categories against the mean Darendeli values provided in Table 6. The residuals provide a measure of the proximity of experimentally measured values to predicted values. As illustrated in Fig. 18, the highest scatter occurs in the medium strain range, while at small and very large strains, the residuals are closely aligned. At small strains (<0.001 %), the residuals are relatively low, indicating a good agreement between the model and experimental data. This is expected as soils exhibit elastic behavior in this range, with minimal differences between disturbed and undisturbed samples due to limited particle rearrangement. In the medium strain range (0.001 %–0.1 %), higher residuals reflect increased data scatter. This is due to soil nonlinearity, fabric and density variations, and differences in sample preparation. Undisturbed samples may retain their inherent structure, whereas reconstituted samples, even when carefully reconstituted, can exhibit slightly altered grain contacts and void ratios, affecting shear modulus predictions. Additionally, soils with FC < 5 % show more scattered residuals as fines act only as void fillers, offering minimal cohesion. For FC > 5 %, fines enhance bonding and plasticity, leading to a more consistent soil response. Similar trends during the elastic-to-nonlinear transition have been reported in previous studies [2,3].

Fig. 19 compares the shear modulus reduction models developed in this study with existing models used in practice. The proposed model effectively captures shear modulus reduction across a wide strain range of up to 10 %, which is not covered by current literature. Significant deviations are observed between the curves from this study and those in the literature. For soils with FC > 5 %, the mean curve is close to Seed and Idriss curve and slightly above Vucetic and Dobry curve for a Plasticity Index of 0. The mean curve for soils with FC > 5 % lies below that for soils with FC < 5 %. The EPRI curves predict delayed nonlinearity, while the curves proposed by Refs. [1,10] predict early strength loss, resulting in overestimation and underestimation of stiffness for the tested soils. The curves from Refs. [1,10] lie significantly below the proposed curves, and those by Refs. [3,14,50], making them unsuitable for seismic response analysis of Indian Himalayan region soils.

The models developed in this study are applicable for effective confining pressures ranging from 60 kPa to 1000 kPa, plasticity indices

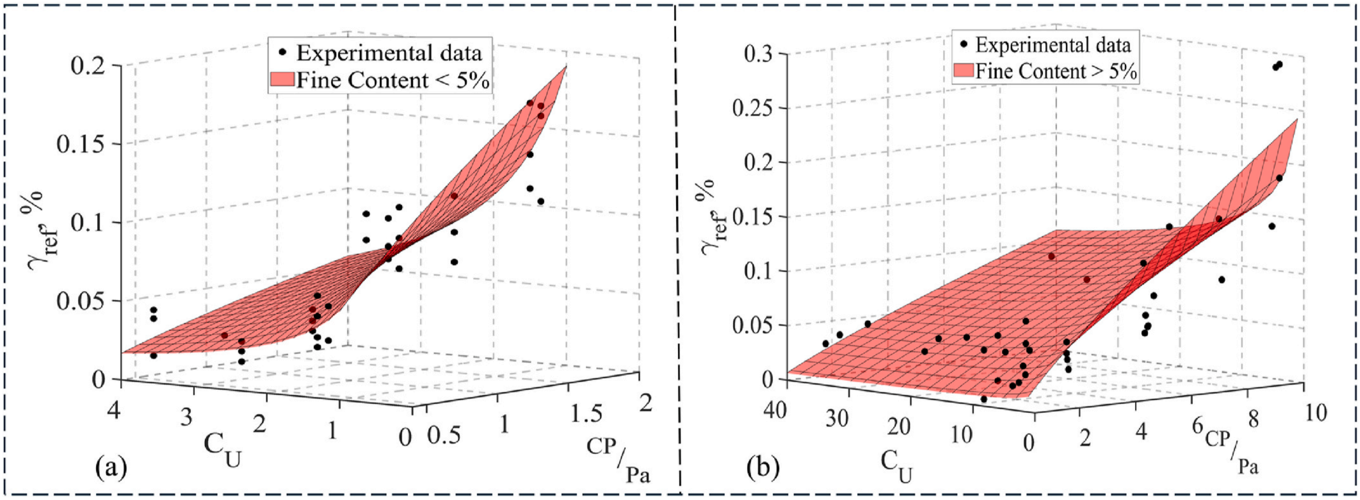

Fig. 15. Multiple regression model for 'γ_{ref}' for soils with fine content (F_C): (a) less than 5 % and (b) greater than 5 % and plasticity index less than 15.

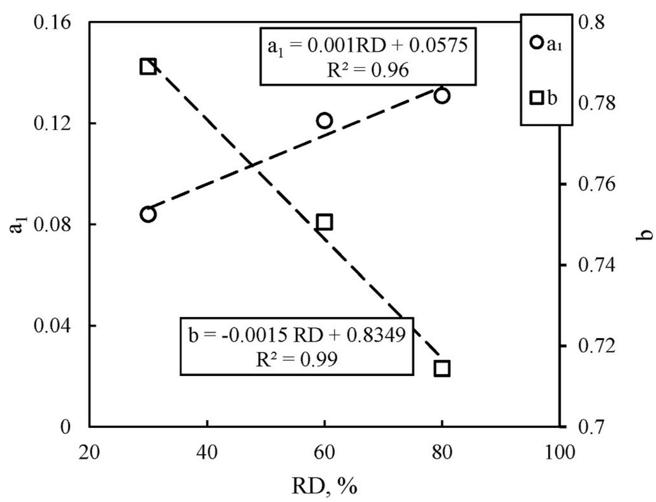

Fig. 16. Dependence of regression 'a_1' and 'b' on relative density (RD).

Table 6
Darendeli's parameters for mean, maximum and minimum curves for soils with fine content (F_C) less than 5 % and with F_C greater than 5 % and having plasticity index (PI) less than 15.

—	Soils with $F_C < 5$ % ($R^2 = 0.96$, RMSE = 0.071)			Soils with $F_C > 5$ % ($R^2 = 0.97$, RMSE = 0.059)		
	Min	*Mean*	*Max*	*Min*	*Mean*	*Max*
γ_{ref}	0.010	0.065	0.300	0.020	0.039	0.150
a	0.620	0.693	0.750	0.720	0.770	0.750

from non-plastic to 15, and coefficients of uniformity from 1.5 to 40. With known soil properties such as relative density, effective confining pressure, and coefficient of uniformity, the reference strain can be easily predicted (Table 5), with the parameter 'a' from Darendeli's model ranging from 0.5 to 0.9. Thus, this study provides two types of models: (1) mean, upper, and lower normalized shear modulus curves for use when information on relative density, depth, and soil gradation (coefficient of uniformity) is lacking, and (2) methods to estimate the 'Reference Strain, γ_{ref}' and 'Curvature Coefficient, a' from Darendeli's model when these properties are known, enabling the prediction of shear modulus at different depths for varying sand gradations.

6. Conclusions

This study presents a detailed experimental investigation and empirical analysis of the shear modulus reduction behavior of various Indian soils across a wide strain range. A combined approach is employed, utilizing resonant column and cyclic triaxial tests on a single specimen. Resonant column tests were conducted for strains ranging from 0.0001 % to 0.05 %, while cyclic triaxial tests were performed for strains ranging from 0.05 % to 10 %. The use of a single specimen for both small and large strain testing is emphasized, as it enhances the reliability of the results and minimizes the variability typically associated with testing multiple specimens. The key conclusions drawn from this research are as follows:

1. The shear moduli (G_1, G'_1, G_2, G_3) calculated from different elastic moduli (E_1, E'_1, E_2, E_3) exhibit significant deviations, especially at larger strains. As strain increases, the asymmetry in the hysteresis loop becomes more pronounced, leading to considerable deviations in shear modulus estimation. Specifically, the shear modulus calculated using both tensile and compressive moduli (E_2 or E_3) deviates by 25 %–130 % from that calculated using only the compressive modulus (E_1). Therefore, E_2 (or E_3) is recommended for more accurate shear modulus calculations, as it better accounts for this asymmetry.
2. The variation in shear modulus with strain is minimal and consistent across both combined (RC and CTX) and separate CTX testing modes. However, differences in sample preparation can significantly affect the results. Therefore, combined testing using the single specimen is recommended to minimize errors in developing modulus reduction curves for a wide strain range.
3. Confining pressure and relative density significantly influence the shear modulus reduction curve. Higher confining pressures and greater relative densities result in increased stiffness. Specifically, higher confining pressures shift the normalized modulus reduction curve to the right, indicating a reduced rate of modulus reduction. However, the effect of relative density on the normalized reduction curve is minimal.
4. The normalized shear modulus reduction data significantly deviates from existing curves used for site response analysis in the literature; particularly, for soils with fines content (FC) < 5 %, compared to those with FC > 5 %.
5. Nonlinear regression analysis using Darendeli's model indicates that parameter a ranges from 0.5 to 0.9 and is independent of confining pressure (CP), coefficient of uniformity (C_U), and relative density (RD). In contrast, the reference strain (γ_{ref}) is strongly influenced by

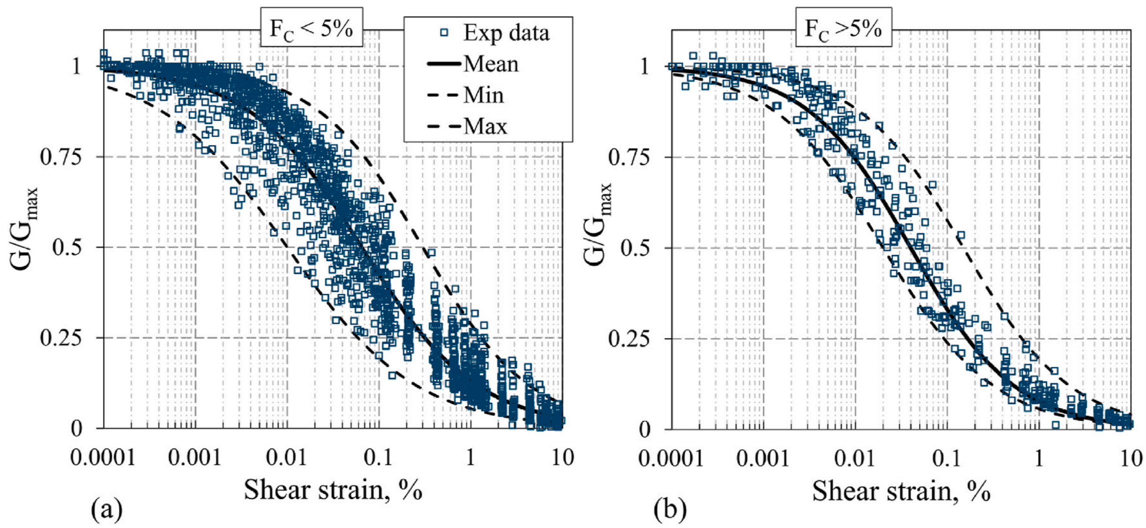

Fig. 17. Mean, minimum, and maximum Darendeli (2001) curves for soils with fine content, (a) less than 5 %, and (b) greater than 5 %.

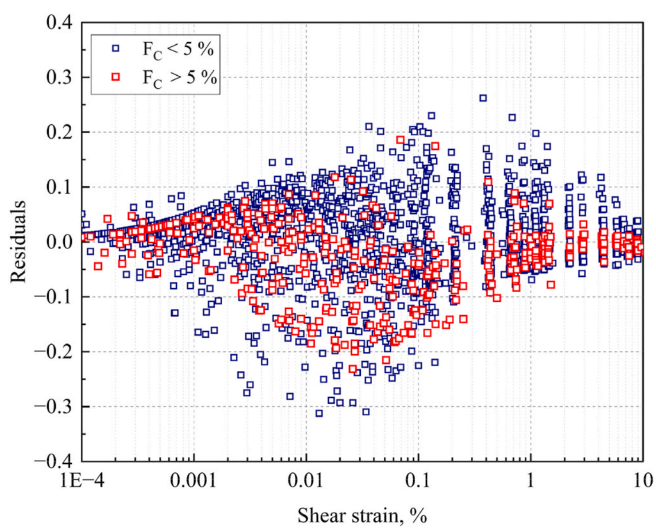

Fig. 18. Residual measured for soils with $F_C < 5$ % and soils with $F_C > 5$ %.

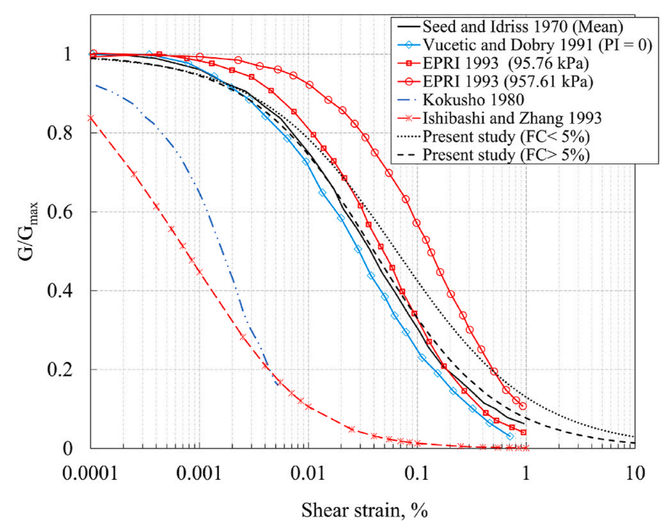

Fig. 19. Comparison of normalized modulus reduction curves developed in the present study with commonly used models/curves in nonlinear site response analysis.

CP and C_U, with higher values indicating greater stiffness in poorly graded soils under increased confining pressures. Further, multiple regression indicated that γ_{ref} follows a power law model. For soils with FC < 5 %, γ_{ref} is influenced by relative density, while for FC > 5 %, it does not.

6. A new shear modulus reduction model is proposed for soils with FC < 5 % and FC > 5 %. This model addresses limitations in existing G estimation methods, reduces sample disturbance using combined RC & CTX testing, and is based on specific test data. Two model types are introduced: (1) mean, upper and lower normalized shear modulus curves for cases where void ratio, depth, and coefficient of uniformity are unknown, and (2) a model to estimate γ_{ref} and a, in the Darendeli's model when these properties are known, allowing predictions of shear modulus at various depths and gradations. Unlike existing models, these new models can predict shear modulus reduction beyond 1 % shear strain. These models can be integrated into geotechnical numerical analyses for geo-structures built on alluvial and deltaic soil deposits, common in India, South Asia and similar regions. This integration will enhance predictions of soil response and deformation, improving the design and performance of various engineering applications.

CRediT authorship contribution statement

P. Anbazhagan: Writing – review & editing, Validation, Supervision, Resources, Methodology, Funding acquisition, Conceptualization. **Kunjari Mog:** Writing – review & editing, Formal analysis, Data curation, Conceptualization. **Mir Zeeshan Ali:** Writing – review & editing, Writing – original draft, Validation, Investigation, Formal analysis, Data curation. **B Sai Laxman:** Writing – review & editing, Investigation.

Declaration of generative AI and AI-assisted technologies in the writing process

During the preparation of this work the author(s) used ChatGPT in order to improve language and readability, only. After using this tool/service, the author(s) reviewed and edited the content as needed and take(s) full responsibility for the content of the publication.

Declaration of competing interest

The authors declare that they have no known competing financial interests or personal relationships that could have appeared to influence the work reported in this paper.

Acknowledgements

This work was supported by the Board of Research in Nuclear Sciences (BRNS) of the Department of Atomic Energy (DAE), Government of India, under the project titled “Probabilistic Seismic Hazard Analysis of Vizag and Tarapur Considering Regional Uncertainties” (Ref No. 36 (2)/14/16/2016-BRNS).

Data availability

Data will be made available on request.

References

[1] Kokusho T. Cyclic triaxial test of dynamic soil properties for wide strain range. Soils Found 1980;20:45–60. https://doi.org/10.3208/SANDF1972.20.2_45.
[2] Darendeli M. Development of a new family of normalized modulus reduction and material damping curves. The University of Texas at Austin; 2001.
[3] Vucetic M, Dobry R. Effect of soil plasticity on cyclic response. J. Geotech. Eng. 1991;117:89–107. https://doi.org/10.1061/(ASCE)0733-9410(1991)117:1(89).
[4] Okur DV, Ansal A. Stiffness degradation of natural fine grained soils during cyclic loading. Soil Dynam Earthq Eng 2007;27:843–54. https://doi.org/10.1016/J.SOILDYN.2007.01.005.
[5] Price AB, DeJong JT, Boulanger RW. Cyclic loading response of silt with multiple loading events. J Geotech Geoenviron Eng 2017;143. https://doi.org/10.1061/(ASCE)GT.1943-5606.0001759.
[6] Zhuang H, Wang R, Chen G, Miao Y, Zhao K. Shear modulus reduction of saturated sand under large liquefaction-induced deformation in cyclic torsional shear tests. Eng Geol 2018;240:110–22. https://doi.org/10.1016/J.ENGGEO.2018.04.018.
[7] Anbazhagan P, Prabhu G, Moustafa Sayed S, Arifi ANS, Aditya P. Provisions for geotechnical aspects and soil classification in Indian seismic design code IS-1893. Disaster Adv 2014;7.
[8] Anbazhagan P, Prabhakaran A, Madhura H, Moustafa SSR, Al-Arifi NSN. Selection of representative shear modulus reduction and damping curves for rock, gravel and sand sites from the KiK-Net downhole array. Nat Hazards 2017;88:1741–68. https://doi.org/10.1007/S11069-017-2944-X.
[9] Bajaj K, Anbazhagan P. Identification of shear modulus reduction and damping curve for deep and shallow sites: kik-Net Data. J Earthq Eng 2019;25:2668–96. https://doi.org/10.1080/13632469.2019.1643807.
[10] Ishibashi I, Zhang X. Unified dynamic shear moduli and damping ratios of sand and clay. Soils Found 1993;33:182–91. https://doi.org/10.3208/SANDF1972.33.182.
[11] Zhang J, Andrus RD, Juang CH. Normalized shear modulus and material damping ratio relationships. J Geotech Geoenviron Eng 2005;131:453–64. https://doi.org/10.1061/(ASCE)1090-0241(2005)131:4(453).
[12] Payan M, Senetakis K. Effect of anisotropic stress state on elastic shear stiffness of sand–silt mixture. Geotech Geol Eng 2019;37:2237–44. https://doi.org/10.1007/s10706-018-0690-9.
[13] Menq FY. Dynamic properties of sandy and gravelly soils. The University of Texas at Austin; 2003.
[14] Seed HB, Idriss IM. Soil moduli and damping factors. Report: EERC 70-10; 1970.
[15] Rohilla S, Sebastian R. Resonant column and cyclic torsional shear tests on Sutlej river sand subjected to the seismicity of Himalayan and Shivalik hill ranges: a case study. Soil Dynam Earthq Eng 2023;166. https://doi.org/10.1016/J.SOILDYN.2023.107766.
[16] Wichtmann T, Triantafyllidis T. Effect of uniformity coefficient on G/Gmax and damping ratio of uniform to well-graded quartz sands. J Geotech Geoenviron Eng 2013;139:59–72. https://doi.org/10.1061/(asce)gt.1943-5606.0000735.
[17] Matasovic N, Ordonez G. D-MOD2000–A computer program for seismic site response analysis of horizontally layered soil deposits, earthfill dams and solid waste landfills. 2012.
[18] Schnabel P. SHAKE, A computer program for earthquake response analysis of horizontally layered sites. 1975.
[19] Hashash Y, Musgrove M, Harmon J, Groholski D, Phillips C, Park D. Deepsoil 2012: 1–107.
[20] Hardin BO, Drnevich VP. Shear modulus and damping in soils: design equations and curves. J Soil Mech Found Div 1972;98:667–92. https://doi.org/10.1061/jsfeaq.0001760.
[21] Kiku H, Yoshida N. Dynamic deformation property tests at large strains. 12th world conference on earthquake engineering. 2000.
[22] Suetomi I, Yoshida N. Nonlinear behavior of surface deposit during the 1995 Hyogoken-Nambu earthquake. Soils Found 1998;38:11–22. https://doi.org/10.3208/SANDF.38.SPECIAL_11.
[23] Miura S, Toki S. A sample preparation method and its effect on static and cyclic deformation-strength properties of sand. Soils Found 1982;22:61–77. https://doi.org/10.3208/SANDF1972.22.61.
[24] Wood FM, Yamamuro JA, Lade PV. Effect of depositional method on the undrained response of silty sand. Can Geotech J 2008;45:1525–37. https://doi.org/10.1139/T08-079/ASSET/IMAGES/LARGE/T08-079F14.JPEG.
[25] Rollins KM, Evans MD, Diehl NB. III WDD. Shear modulus and damping relationships for gravels. J Geotech Geoenviron Eng 1998;124:396–405. https://doi.org/10.1061/(ASCE)1090-0241(1998)124:5(396).
[26] Cevik A, Cabalar AF. Modelling damping ratio and shear modulus of sand–mica mixtures using genetic programming. Expert Syst Appl 2009;36:7749–57. https://doi.org/10.1016/J.ESWA.2008.09.010.
[27] Senetakis K, Anastasiadis A, Pitilakis K. Dynamic properties of dry sand/rubber (SRM) and gravel/rubber (GRM) mixtures in a wide range of shearing strain amplitudes. Soil Dynam Earthq Eng 2012;33:38–53. https://doi.org/10.1016/J.SOILDYN.2011.10.003.
[28] Senetakis K, Anastasiadis A, Pitilakis K. Normalized shear modulus reduction and damping ratio curves of quartz sand and rhyolitic crushed rock. Soils Found 2013;53:879–93. https://doi.org/10.1016/J.SANDF.2013.10.007.
[29] Oztoprak S, Bolton MD. Stiffness of sands through a laboratory test database. Geotechnique 2013;63:54–70. https://doi.org/10.1680/GEOT.10.P.078.
[30] Amir-Faryar B, Aggour MS, McCuen RH. Universal model forms for predicting the shear modulus and material damping of soils. Geomechanics Geoengin 2017;12:60–71. https://doi.org/10.1080/17486025.2016.1162332.
[31] Kumar SS, Krishna AM, Dey A. Evaluation of dynamic properties of sandy soil at high cyclic strains. Soil Dynam Earthq Eng 2017;99:157–67. https://doi.org/10.1016/J.SOILDYN.2017.05.016.
[32] Park D, Kishida T. Shear modulus reduction and damping ratio curves for earth core materials of dams. Can Geotech J 2019;56:14–22. https://doi.org/10.1139/CGJ-2017-0529/ASSET/IMAGES/LARGE/CGJ-2017-0529F7.JPEG.
[33] ASTM D7928-21e1. Standard test method for particle-size distribution (gradation) of fine-grained soils using the sedimentation (hydrometer) analysis. West Conshohocken, PA: ASTM International; 2021.
[34] ASTM D2216-19. Standard test methods for laboratory determination of water (moisture) content of soil and rock by mass. West Conshohocken, PA: ASTM International; 2019.
[35] ASTM D7263-21. Standard test methods for laboratory determination of density and unit weight of soil specimens. West Conshohocken, PA: ASTM International; 2021.
[36] ASTM D4318-17. Standard test methods for liquid limit, plastic limit, and plasticity index of soils. West Conshohocken, PA: ASTM International; 2017.
[37] ASTM D4253-16e1. Standard test methods for maximum index density and unit weight of soils using a vibratory table. West Conshohocken, PA: ASTM International; 2019.
[38] Lade P, Liggio C, Yamamuro J. Effects of non-plastic fines on minimum and maximum void ratios of sand. Geotech Test J 1998. https://doi.org/10.1520/GTJ11373J.
[39] Mog K, Anbazhagan P. Dynamic properties of surface liquefied site silty-sand of Tripura, India. Sustainable civil infrastructures. Springer Science and Business Media B.V; 2019. p. 140–54. https://doi.org/10.1007/978-3-030-01920-4_12.
[40] Mog K, Anbazhagan P. Evaluation of the damping ratio of soils in a resonant column using different methods. Soils Found 2022;62. https://doi.org/10.1016/J.SANDF.2021.101091.
[41] Saxena SK, Reddy KR. Dynamic moduli and damping ratios for Monterey no. 0 sand by resonant column tests. Soils Found 1989;29:37–51. https://doi.org/10.3208/SANDF1972.29.2_37.
[42] Chen G, Zhou Z, Sun T, Wu Q, Xu L, Khoshnevisan S, et al. Shear modulus and damping ratio of sand–gravel mixtures over a wide strain range. J Earthq Eng 2019;23:1407–40. https://doi.org/10.1080/13632469.2017.1387200.
[43] Qin Y, Ma W, Xu Z, Chen G, Zhao K, Wu Q. Effects of consolidation conditions on the dynamic shear modulus of saturated coral sand over a wide strain range. Eng Geol 2023;324:107260. https://doi.org/10.1016/J.ENGGEO.2023.107260.
[44] Vucetic M, Mortezaie A. Cyclic secant shear modulus versus pore water pressure in sands at small cyclic strains. Soil Dynam Earthq Eng 2015;70:60–72. https://doi.org/10.1016/J.SOILDYN.2014.12.001.
[45] Mog K. Deformation characteristics of soil under sequential dynamic torsional and cyclic axial loading. Bangalore: Indian Institute of Science (IISc); 2022.
[46] Seed HB, Wong RT, Idriss IM, Tokimatsu K. Moduli and damping factors for dynamic analyses of cohesionless soils. J. Geotech. Eng. 1986;112:1016–32. 10.1061/(ASCE)0733-9410(1986)112:11(1016).
[47] Dammala PK, Krishna AM, Bhattacharya S, Nikitas G, Rouholamin M. Dynamic soil properties for seismic ground response studies in Northeastern India. Soil Dynam Earthq Eng 2017;100:357–70. https://doi.org/10.1016/J.SOILDYN.2017.06.003.
[48] Chung R, Yokel F, Drnevich V. Evaluation of dynamic properties of sands by resonant column testing. Geotech Test J 1984;7:60–9. https://doi.org/10.1520/GTJ10594J.
[49] Wichtmann T, Triantafyllidis T. Influence of a cyclic and dynamic loading history on dynamic properties of dry sand, part I: cyclic and dynamic torsional prestraining. Soil Dynam Earthq Eng 2004;24:127–47. https://doi.org/10.1016/J.SOILDYN.2003.10.004.
[50] EPRI. Guidelines for determining design basis ground motions, Final report. Palo Alto, CA: EPRI TR-102293; 1993.
[51] Kondner RL. Hyperbolic stress-strain response: cohesive soils. J Soil Mech Found Div 1963;89:115–43. https://doi.org/10.1061/JSFEAQ.0000479.
[52] Duncan JM, Chang C-Y. Nonlinear analysis of stress and strain in soils. J Soil Mech Found Div 1970;96:1629–53. https://doi.org/10.1061/JSFEAQ.0001458.
[53] Vardanega PJ, Bolton MD. Stiffness of clays and silts: normalizing shear modulus and shear strain. J Geotech Geoenviron Eng 2013;139:1575–89. https://doi.org/10.1061/(ASCE)GT.1943-5606.0000887.
[54] Stokoe K, Darendeli M, Andrus RD. Dynamic soil properties: laboratory, field and correlation studies. Earthquake Geotech Eng 1999:811–45.